1   **An assessment of latest Cretaceous *Pycnodonte vesicularis* (Lamarck, 1806) shells as records for**
2   **palaeoseasonality: A multi-proxy investigation**

3   de Winter, Niels J.*[1], Vellekoop, Johan*[1,2], Vorsselmans, Robin[2], Golreihan, Asefeh[2], Soete, Jeroen[2],
4   Petersen, Sierra V.[3], Meyer, Kyle W.[3], Casadio, Silvio[4], Speijer, Robert P.[2], Claeys, Philippe[1]

5   *[1]Analytical, Environmental and Geo-Chemistry (AMGC), Vrije Universiteit Brussel (VUB), Brussels,*
6   *Belgium.*
7   *[2]Department of Earth and Environmental Science, KU Leuven, Heverlee, Belgium*
8   *[3]Earth and Environmental Sciences Department, University of Michigan, Ann Arbor, Michigan, USA.*
9   *[4] Escuela de Geología, Paleontología y Enseñanza de las Ciencias, Universidad Nacional de Río Negro,*
10   *CONICET, General Roca, Argentina.*

11

12   *Niels J. de Winter and Johan Vellekoop contributed equally to this work

13

14   Corresponding author: niels.de.winter@vub.be

15

16   **Abstract**

17   In order to assess the potential of the honeycomb oyster *Pycnodonte vesicularis* for the
18   reconstruction of palaeoseasonality, several specimens recovered from late Maastrichtian strata in
19   the Neuquén Basin (Argentina) were subject to a multi-proxy investigation, involving scanning
20   techniques, trace element and isotopic analysis. Combined CT scanning and light microscopy reveals
21   two calcite microstructures in *P. vesicularis* shells (vesicular and foliated calcite). Micro-XRF analysis
22   and cathodoluminescence microscopy show that reducing pore fluids were able to migrate through
23   the vesicular portions of the shells (aided by bore holes) and cause recrystallization of the vesicular
24   calcite. This renders the vesicular portions not suitable for palaeoenvironmental reconstruction. In
25   contrast, stable isotope and trace element compositions show that the original chemical
26   composition of the foliated calcite is well-preserved and can be used for the reconstruction of
27   palaeoenvironmental conditions. Stable oxygen and clumped isotope thermometry on carbonate
28   from the dense hinge of the shell yield sea water temperatures of 11°C, while previous TEX$_{86}^H$
29   palaeothermometry yielded much higher temperatures. The difference is ascribed to seasonal bias
30   in the growth of *P. vesicularis*, causing warm seasons to be underrepresented from the record, while
31   TEX$_{86}^H$ palaeothermometry seems to be biased towards warmer surface water temperatures. The
32   multi-proxy approach employed here enables us to differentiate between well-preserved and
33   diagenetically altered portions of the shells and provides an improved methodology for
34   reconstructing palaeoenvironmental conditions in deep time. While establishing a chronology for
35   these shells was complicated by growth cessations and diagenesis, cyclicity in trace elements and
36   stable isotopes allowed for a tentative interpretation of the seasonal cycle in late Maastrichtian
37   palaeoenvironment of the Neuquén basin. Attempts to independently verify the seasonality in sea
38   water temperature by Mg/Ca ratios of shell calcite are hampered by significant uncertainty due to
39   the lack of proper transfer functions for pycnodontein oysters. Future studies of fossil ostreid
40   bivalves should target dense foliated calcite rather than sampling bulk or vesicular calcite. Successful
41   application of clumped isotope thermometry on fossil bivalve calcite in this study indicates that
42   temperature seasonality in fossil ostreid bivalves may be constrained by the sequential analysis of
43   well-preserved foliated calcite samples using this method.

44

1. Introduction

46 The Late Cretaceous is generally considered a greenhouse world (e.g. Hay, 2008). Indeed,
47 reconstructed global mean temperatures and atmospheric pCO_2 concentrations for this period
48 generally exceed those of the present-day climate (e.g., Berner, 1990; Andrews et al., 1995; Ekart et
49 al., 1999; Hunter et al., 2008; Quan et al., 2009; Wang et al., 2013). As such, the Late Cretaceous may
50 be considered an analogue for climate of the near future if anthropogenic greenhouse gas emissions
51 continue unabated (Hay, 2013; IPCC, 2014; Dlugokencky, 2017). Many studies have yielded
52 reconstructions of Late Cretaceous climates using either climate models or a variety of proxies in
53 temporally long archives, such as deep-sea cores and continental sections (Pearson et al., 2001;
54 Huber et al., 2002; Otto-Bliesner et al., 2002; Miller et al., 2003; Friedrich et al., 2012; de Winter et
55 al., 2014; Vellekoop et al., 2016). Yet, although most deep-time climate reconstructions so far have
56 focused on reconstructing mean annual temperatures (MAT), climate change also involves changes
57 in other climate parameters, such as precipitation, seasonality and the frequency of extreme
58 weather events, which all take place on timescales shorter than those that can be resolved in the
59 above mentioned long archives. Therefore, it is important that these climate variations are
60 understood on a shorter timescale.

61 One way to achieve such high-resolution palaeoclimate and palaeoenvironmental reconstructions is
62 by using marine organisms that grow their shells incrementally. Marine bivalves are excellent
63 palaeoclimate recorders, since they have a broad geographic distribution and because the rapid
64 secretion of their shells allows for the high time resolution needed to resolve climate parameters on
65 a sub-annual scale (e.g. Jones, 1983; Dettman and Lohmann, 1993; Steuber, 1996; Schöne et al.,
66 2005a;b). The relationship between shell chemistry and the environmental conditions in which
67 bivalves grow has been studied intensively (Gillikin et al., 2005a; Elliot et al., 2009; Marali and
68 Schöne, 2015). As a result, many geochemical proxies have been described based on bivalve calcite.
69 Examples include temperature calibrations for Mg/Ca and stable oxygen isotope ratios ($\delta^{18}O$; e.g.
70 Klein et al., 1996a; Richardson et al., 2004; Freitas et al., 2008; Wanamaker et al., 2008), tentative
71 salinity calibrations using Sr/Ca and the combination of Mg/Ca and $\delta^{18}O$ (Dodd and Crisp, 1982; Klein
72 et al., 1996a; Watanabe et al., 2001) and proxies for palaeoproductivity, such as Ba/Ca and Mn/Ca
73 (Lazareth et al., 2003; Gillikin et al., 2008).

74 Despite their potential for high-resolution palaeoenvironmental reconstruction, seasonally resolved
75 bivalve records are rarely combined with longer timescale reconstructions (e.g. Steuber et al., 2005;
76 Schöne et al., 2005c; Harzhauser et al., 2011; Butler et al., 2013; Hallmann et al., 2013). A
77 disadvantage of using bivalve records for long-term palaeoclimate reconstructions is the potential
78 problems that arise when using multiple bivalve species for palaeoclimate reconstruction (Gillikin et
79 al., 2005a; b; de Winter et al., 2017a). Culture experiments in extant bivalve species have shown that
80 palaeoenvironmental proxies in bivalve calcite may be affected by mechanisms that are independent
81 of the environment of the animal and are controlled by parameters such as growth, reproductive
82 cycle and metabolism (the so-called "vital effects"; Dunbar and Wefer, 1984; Weiner and Dove,
83 2003; Gillikin et al., 2005b; Lorrain et al., 2005; Carré et al., 2005). These vital effects are often
84 species-specific and limit the applicability of proxy transfer functions from modern culture studies to
85 multiple species in the same study or to species for which no culture study data is available. The
86 integration of different species of bivalves in palaeoclimate studies is further complicated by the
87 various ecological niches these species of bivalves occupy, resulting in great variability in their direct
88 environments (Chauvaud et al., 2005; Dreier et al., 2014). In addition, bivalves are often, though not
89 exclusively, found in shallow marine and estuarine environments. This further complicates the

2

90   interpretation of bivalve records in terms of global climate (e.g. Surge et al., 2001, Richardson et al.,
91   2004; Gillikin et al., 2008; Wisshak et al., 2009; Ullmann et al., 2010; Crippa et al., 2016), as these
92   environments are often characterized by large variations in temperature, salinity and water
93   chemistry, making it hard to disentangle the effects of different environmental parameters on
94   geochemical proxies (e.g. Duinker et al., 1982; Morrison et al., 1998; Pennington et al., 2000).

95   The above-mentioned problem of combining different high-resolution climate records to study
96   climatic variations on a geological timescale can be overcome by combining results from multiple
97   well-preserved bivalve specimens of the same species and in the same geological setting. Several
98   studies have tried such a multi-specimen approach to trace changes in high-resolution climate
99   parameters, such as seasonal variations, over geological timescales (Dettman and Lohmann, 2000;
100   Dettman et al., 2001; Steuber et al., 2005; Gutiérrez-Zugasti et al., 2016). However, such
101   reconstructions require bivalve species that preserve well, are geographically widespread, have a
102   high occurrence frequency over longer timescales and record seasonal-scale variations within their
103   shell.Potential candidate species for such studies are bivalves of the genus *Pycnodonte*. This genus of
104   oysters (Bivalvia: Ostreoida; Fischer von Waldheim, 1835) is characterized by a well-developed
105   commissural shelf and vesicular shell microstructure (hence the name "honeycomb oyster" or "foam
106   oyster"; Stenzel, 1971; Hayami and Kase, 1992). Members of the genus *Pycnodonte* are found in
107   geological deposits from the Lower Cretaceous to the Pleistocene. The appearance of *Pycnodonte*
108   shells in a wide range of palaeolatitudes and geological settings, especially in the Cretaceous, makes
109   them a promising archive for high-resolution climate reconstructions (Ayyasami, 2006; Fossilworks,
110   2017). As mentioned in Titschak et al. (2010), records from large and long-living bivalves, such as
111   *Pycnodonte*, provide several advantages in comparison with other seasonality archives. They are
112   slow-growing in comparison to other ostreid taxa, have rather limited kinetic effects and
113   disequilibrium fractionation of stable isotopes (McConnaughey 1989; Abele et al., 2009). In addition,
114   *Pycnodonte* bivalves likely did not have symbionts, in contrast to, for example, tridacnid bivalves
115   (Elliot et al., 2009). This means that *Pycnodonte* bivalves take up nutrients and other elements
116   directly from their environment, simplifying the interpretation of their shell composition. Their low-
117   Mg calcite shells are less prone to diagenetic alteration than shells made of aragonite or high-Mg
118   calcite (Al-Aasm and Veizer, 1986; Pirrie and Marshall, 1990), and their sedentary life mode ensures
119   that they fossilize in life position. The latter enables the integration of environmental information
120   extracted from the sediments in which they are fossilized into the discussion of their shell chemistry.

121   The species *Pycnodonte vesicularis* (Lamarck, 1806) is one of the most common and long-ranging
122   species of *Pycnodonte.* Therefore, in this study the potential for *P. vesicularis* to be used as a record
123   for sub-annual environmental variability in the Late Cretaceous is explored. The present study
124   focuses on the characteristics of fossil specimens of *P. vesicularis* from the upper Maastrichtian
125   Jagüel Formation of the Bajada de Jagüel section, Argentina (**Figure 1A**). A range of qualitative, semi-
126   quantitative and quantitative methods is applied to investigate the nature of the *P. vesicularis* shell
127   material, shell morphology and its preservation state. The aim of this multi-proxy approach is to
128   characterize the microstructure and chemical composition of the *P. vesicularis* shell and its
129   ontogenetic development and to assess its potential as a recorder of palaeoseasonality.

130

131   **2. The species *Pycnodonte vesicularis***

132   *Pycnodonte vesicularis* was reclining and inhabited muddy bottoms on the shallow marine shelf with
133   a low sedimentation rate (e.g. Brezina et al., 2014). Individual valves of *P. vesicularis* vary
134   considerably in dimension, outline, convexity, wall thickness, muscle scar position, deepness and

shape, as well as the characteristics of chomata (Pugaczewska, 1977; Brezina et al., 2014). This variability depends on the age of the individual and local environmental conditions, especially the substrate. According to Berzina et al. (2014), about one third of *P. vesicularis* valves at Bajada de Jagüel are mature (gerontic) specimens, characterized by relatively thick valves (>10mm) with a well-developed vesicular layer. Given their longer life span, mature specimens of *P. vesicularis* were considered most suitable for the present investigation.

In the past, several studies have attempted to calculate the age of individuals of *P. vesicularis* based on the number of laminae in the complex of lamellar and vesicular layers (Nestler, 1965), or the number of growth lines in the ligament (Müller, 1970). Yet, so far no studies have investigated the potential of *P. vesicularis* shells as palaeoseasonality records based on their geochemical signature. Unfortunately, no extant species of *Pycnodonte* are known, rendering culture experiments for these species impossible. However, two species of the closely related *Neopycnodonte* (Stenzel, 1971) are found in deep-sea habitats today (*Neopycnodonte conchlear*, Poli, 1795, and *Neopycnodonte zibrowii*; Videt, 2004; Wisshak et al., 2009), whereas the extant pycnodontein genus *Hyotissa* is characterized by a shallow-marine distribution (Titschack et al., 2010). Detailed studies of the shell morphology and chemical composition of *N. zibrowii* and *Hyotissa hyotis* were reported in Wisshak et al., (2009) and Titschak et al., (2010), respectively, and are used as a basis for comparison of the *Pycnodonte* oyster shells.

3. Geological Background

3.1 Paleogeographical context

The studied specimens were collected from the Bajada de Jagüel (BJ) section (38°06'10.5"S, 68°23'20.5"W). The site is situated in the Neuquén Basin in Argentina, which is bordered to the south by the North Patagonian massif and to the northeast by the Sierra Pintada massif (**Figure 1B and 1C**). The Bajada de Jagüel section has a palaeolatitude of ~43˚S ± 2° relative to the palaeomagnetic reference frame of Torsvik et al. (2012) according to palaeolatitude.org (van Hinsbergen et al., 2015). A large transgression from the South Atlantic into the basin (Bertels, 2013) occurred from the late Maastrichtian to early Danian, during a time of relative tectonic quiescence and low magmatic activity (Malumian et al., 2011).

3.2 Palaeoenvironment

The Maastrichtian mudstones of the Jagüel Fm. are homogeneous and intensely bioturbated, indicating a well-oxygenated seafloor, with palaeodepths of approximately 50-75 m (Scasso et al., 2005; Woelders et al., 2017; see also **Figure 1**). A coarse-grained, mottled, clayey sandstone bed, 15-25 cm thick, separates the Maastrichtian and Danian mudstones. This sandstone bed represents the K-Pg boundary and is thought to have resulted from a tsunami wave, related to the Chicxulub impact event (Scasso et al., 2005). During the late Maastrichtian and early Danian, North and Central Patagonia experienced a warm, humid climate. Pollen records suggest rainforests, coastal mangrove forests and swamp communities in the region (Baldoni, 1992; Kiessling et al., 2005; Barreda and Palazzesi, 2007; Iglesias et al., 2007; Palazzesi and Barreda, 2007). This vegetation type is classified as megathermal and indicates average air temperature of 24°C or higher (Barreda and Palazzesi, 2007; Palazzesi and Barreda, 2007; Barreda et al., 2012). Average annual sea surface temperatures are estimated to have been 26-29°C in the latest Maastrichtian at Bajada de Jagüel, based on TEX_{86}^H-palaeothermometry (Woelders et al., 2017; **Figure 1D**). An average of these TEX_{86}^H-temperatures weighted to the stratigraphic abundance of *P. vesicularis* (Aberhan and Kiessling, 2014) yields a

179 temperature of 27.3°C ± 2.5°C for the environment of *P. vesicularis* in the Bajada de Jagüel formation
180 (see **suppl_Weighted_TEX**). While hypersaline conditions have been inferred for the northernmost
181 part of the Neuquén Basin, the central part of the Neuquén Basin, where the BJ site is located, is
182 suggested to have experienced more normal marine conditions. The latter is evidenced by the
183 presence of planktic foraminifera, dinocysts and relatively few terrestrial palynomorphs (Prámparo
184 et al., 1996; Prámparo and Papú 2006; Woelders et al., 2017). Yet, Woelders et al. (2017) inferred
185 enhanced runoff and stratification of the water column at the Bajada de Jaguël site during the late
186 Maastrichtian warming (450-150 kyr before the K-Pg boundary). Hence, salinity may have deviated
187 from normal marine during the lifetime of the *Pycnodonte* specimens studied here.

188

189 4. Materials and methods

190 4.1 Sample acquisition and preparation

191 Seven specimens of *Pycnodonte vesicularis* were collected from the upper Maastrichtian Jagüel
192 Formation in the Bajada de Jaguël section (**Figure 1**), labelled "M0", "M4", "M5", "M6", "M8",
193 "M10" and "M11". All shells were collected from the upper 5m of below the Cretaceous-Palaeogene
194 boundary (see **Figure 1**). The abundance of *Pycnodonte* in these strata, based on the data of
195 Aberhan and Kiessling (2014), is indicated in **Figure 1**. There is a *Pycnodonte*-bed approximately 50
196 cm below the K-Pg boundary, which is the likely source of most of the specimens. Yet, the specimens
197 studied here were collected as surface finds, so downhill transport cannot be excluded with
198 certainty. Therefore, a more precise stratigraphic position cannot be provided. For associated fauna,
199 see Aberhan et al. (2007), Aberhan and Kiessling (2014) and Woelders et al. (2017).

200 Four of these specimens ("M0", "M4", "M6" and "M11", see **Figure 2**) represent completely
201 preserved left valves of mature specimens of *P. vesicularis* (c.f. Pugaczewska, 1977), while the
202 remaining three ("M5", "M8" and "M10") were incomplete. Specimens were selected that differ
203 from each other in morphology, body size and extent of biodegradation (e.g. bore holes), to assess
204 both the potentials and possible pitfalls of this taxon as a palaeoseasonality recorder. The four
205 complete shells were cleaned and cast into Araldite® 2020 epoxy resin (Araldite, Basel, Switzerland)
206 before being cut along the major growth axis of the shell using a slow rotating rotary saw (Ø 1 mm).
207 A parallel slab was cut out of one half of the shell, while the other half was preserved (archive half).
208 The resulting thick section, with a typical thickness of 4 mm, was polished using a series of
209 progressively higher-grade silicon carbide polishing disks (up to P2400) to allow a smooth surface for
210 sampling and imaging. The three incomplete shells were left untreated and were only used for bulk
211 analysis.

212 4.2 Colour scanning and microscopy

213 Polished surfaces of shell sections were colour-scanned at 6400 dpi (~4 µm resolution) using an
214 Epson 1850 flatbed scanner. Shell microstructures were studied and imaged at 50x magnification
215 using an Olympus BX60 optical microscope (KU Leuven, Belgium). In order to study the preservation
216 of pristine calcite in *P. vesicularis*, shell slabs were studied using cathodoluminescence microscopy
217 using a Technosyn Cold Cathodoluminescence model 8200, mark II microscope operated at 16-20 kV
218 electron gun potential, 420 µA beam current, 0.05 Torr (6.6 * 10^{-5} bar) vacuum and 5 mm beam
219 width (KU Leuven, Belgium). Cathodoluminescence (CL) refers to the emission of light from material
220 during excitation by an electron beam. The wavelength (i.e. colour) of the emitted light depends on
221 the crystal lattice structure and on activators, i.e. light emitting centres constituted by chemical
222 elements or crystal defects. CL microscopic observations of the shell sections thus enable the

223 recognition of crystal defects and evaluation of the preservation state of the shells (e.g. overgrowth,
224 recrystallisation, dissolution), and is used to evaluate whether obtained element concentrations and
225 isotopic ratios reflect the original shell signature (Barbin, 2000).

226 **4.3 Porosity and trace element analysis**

227 In order to visualize shell microstructure and the pore network, high-resolution 3D micro-
228 tomography analysis was carried out on the archive half of *Pycnodonte* specimens using a General
229 Electric Nanotom microCT X-Ray CT scanner (KU Leuven, Belgium). One half shell was scanned at a
230 30 μm spatial resolution while representative shell pieces of interest were scanned at 1.5 μm
231 resolution. The CT images were segmented in Matlab by applying a dual thresholding algorithm. The
232 shell porosity was rendered in 3D and labelled in Avizo Fire 7.0. Pore parameters were calculated in
233 Avizo and Matlab (see **SI_CT_scanning** for details). Micro-XRF measurements were carried out using
234 a Bruker M4 Tornado micro-XRF scanner (AMGC, VUB, Brussels, Belgium). Details on the setup and
235 methodology of the M4 Tornado μXRF scanner can be found in de Winter and Claeys (2016), de
236 Winter et al. (2017b) and in **suppl_XRF_IRMS**. Care was taken to limit sampling to the dense calcite
237 in the hinge of the shells, though observations of the microstructure of the shell hinge show that
238 incorporation of vesicular calcite into the profile could not be fully avoided (see section 5.1.1 and
239 5.1.3).

240 **4.4 Trace elements in bivalves**

241 The use of trace element concentrations in fossil bivalve shells as a means of reconstructing
242 palaeoenvironmental conditions is subject to ongoing debate. As mentioned above, some tentative
243 calibrations have been made that link trace element ratios in shell carbonate to environmental
244 conditions in modern bivalves (e.g. Jones, 1980; Klein et al., 1996a; Freitas et al., 2005; Wanamaker
245 et al., 2008). However, the degree by which the incorporation of these trace element concentrations
246 is controlled by the environment of the bivalve, as opposed to vital effects, is often uncertain (e.g.
247 Weiner and Dove, 2003; Gillikin et al., 2005b; Lorrain et al., 2005). An example is the Mg/Ca ratio,
248 which is thought to reflect the calcification temperature of the shell (e.g. Klein et al., 1996a). While
249 the Mg/Ca palaeothermometer is commonly applied in foraminifera studies (e.g. Ederfield and
250 Ganssen, 2000; Lear et al., 2000), calibrations of this proxy for different bivalve taxa vary widely
251 (Klein et al., 1996a; Vander Putten et al., 2000; Takesue and van Geen, 2004; Freitas et al., 2005;
252 Surge and Lohmann, 2008; Wanamaker et al., 2008; Mouchi et al., 2013; see also de Winter et al.,
253 2017a). Even Mg/Ca calibration curves for oyster species within the same genus (*Crassostrea*
254 *virginica* in Surge and Lohmann (2008) and *Crassostrea gigas* in Mouchi et al. (2013) yield very
255 different results, illustrating that the temperature dependence of Mg/Ca ratios in bivalve calcite is
256 not straightforward. Relationships of bivalve Mg/Ca ratios with temperature are known to break
257 down during periods of growth stress (Lorens and Bender, 1980; Weiner and Dove, 2003; Takesue
258 and van Geen, 2004). Part of the Mg in bivalve shells is associated with organic molecules in the
259 matrix in the shell rather than being substituted for Ca in the crystals of bivalve calcite (Lorens and
260 Bender, 1980). In addition, factors determining incorporation of Mg in bivalve carbonate are partly
261 controlled by physiological processes and are therefore species or even specimen specific (e.g.
262 Freitas et al., 2006; 2008).
263 Another commonly reported ratio, that of Sr/Ca, has been demonstrated to co-vary with changes in
264 growth and metabolic rate in some taxa (Klein et al., 1996b; Gillikin et al., 2005b; Lorrain et al.,
265 2005). However, a few studies have shown a positive correlation with water temperature in other
266 species (e.g. Freitas et al., 2005; Wanamaker et al., 2008). These results are somewhat
267 counterintuitive since the partition coefficient of Sr into calcite is negatively correlated with
268 temperature (Rimstidt et al., 1998). The above shows that the extent of vital effects is highly taxon-
269 specific and that palaeoclimate reconstructions based on trace element records in bivalve shells
270 need to be interpreted with great care.

271 Besides sea water temperature, attempts have been made to reconstruct other environmental
272 parameters, such as redox conditions and palaeoproductivity, based on trace element records in
273 bivalves. Examples of such proxies include elements that are enriched in skeletons of primary
274 producers such as Ba (Gillikin et al., 2008; Marali et al., 2017), redox-sensitive elements like Mn
275 (Freitas et al., 2006) and micronutrients such as Zn and Cd, which are known to be taken up into
276 bivalve shells and whose concentration profiles reflect changes in palaeoproductivity (Carriker et al.,
277 1980a; Calmano et al., 1993; Jackson et al., 1993; Wang and Fisher, 1996; Guo et al., 1997). Seasonal
278 records of these proxies are reproducible between different shells in the same environment (Gillikin
279 et al., 2008). While these proxies have not been explored in detail, their interpretation gives
280 additional information about the ambient sea water chemistry and illustrates the advantage of
281 applying the multi-proxy approach to reconstruct palaeoseasonality from bivalve shells (de Winter et
282 al., 2017a).
283

4.5 Stable isotope analyses

285 Samples for stable isotope analysis were drilled using a microscope-guided Merchantek drill, coupled
286 to Leica GZ6 microscope, equipped with a 300 µm diameter tungsten carbide drill bit. Spatial sample
287 resolutions smaller than the diameter of the drill were obtained by abrading consecutive samples off
288 the side of the sampling front. This was achieved by moving in steps of 100 µm along a ±2 mm wide
289 linear sampling path, oriented parallel to the growth lines of the shell and in the growth direction of
290 the shell (447 measurements in total; see also Van Rampelbergh et al., 2014). Dense foliated calcite
291 in the hinge of the shells was targeted while sampling for stable isotope analysis, but as a result of
292 the shell structure (see discussion below) the incorporation of some vesicular calcite could not
293 always be excluded. Note that, as a consequence of the abrading sampling strategy, the width of the
294 sampling path for IRMS samples is much larger (2 mm) than the width of the sampling path of a
295 µXRF line scan (25 µm). This caused more vesicular calcite to be incorporated into stable isotope
296 measurements than in µXRF measurements, as it was easier to avoid the vesicular microstructure in
297 µXRF line scans.

298 Aliquots of ±50 µg of sampled calcite were allowed to react with 104% phosphoric acid (H_3PO_4) at
299 70°C in a NuCarb carbonate preparation device and stable oxygen and carbon isotope ratios ($\delta^{13}C$
300 and $\delta^{18}O$) were measured using a NuPerspective Isotope Ratio Mass Spectrometer (Nu Instruments
301 Ltd, Wrexham, UK) at the AMGC lab of the VUB. For analytical uncertainties and reproducibiltiy, see
302 **suppl_XRF_IRMS**. All stable isotope values are reported in permille relative to the Vienna Pee Dee
303 Belemnite standard (‰VPDB). While µXRF and IRMS measurements were carried out on the same
304 transect, small differences in the length of the records did occur and these were corrected by
305 linearly rescaling the stable isotope records to match the length of trace element records in the
306 same shell.

4.6 Clumped isotope analysis

308 The stable and clumped isotopic composition of samples from five shells (M4, M5, M8, M10 and
309 M11) was measured at the University of Michigan Stable Isotope Laboratory. Bulk sampling for
310 clumped isotope analysis was carried out in two ways: 1) Slabs of dense calcite were broken off the
311 ventral margin of three shells (M5, M8 and M10) and powdered by hand. 2) Samples were drilled
312 from the dense hinge area of four shells (M4, M5, M8 and M11). Sample preparation was performed
313 on a manual extraction line following Defliese et al. (2015), with the temperature of the Porapak™
314 trap increased to avoid fractionating stable isotope values (Petersen et al., 2016). Aliquots of 3.5-5
315 mg carbonate powder were reacted with phosphoric acid (H_3PO_4) at 75°C and sample CO_2 was
316 analysed on a ThermoFinnegan MAT253 equipped with Faraday cups to measure m/z 44-49. . Data

317 presented in the main manuscript were processed using the Santrock/Gonfiantini parameters
318 (Daëron et al., 2016; Schauer et al., 2016) and the high-temperature composite calibration of
319 Defliese et al. (2015). Further details on the measurement and calibration procedure of clumped
320 isotope thermometry are found in **supplementary data 1**, along with raw data processed using both
321 Santrock/Gonfiantini and Brand parameters.

322

5. Results

5.1 *Pycnodonte vesicularis* shell structure

5.1.1 Shell microstructures

An overview of the results of colour scanning, microscopic analyses and µXRF mapping on specimen
M11 reveals the microstructure of the shells (**Figure 3; supplementary data 2,
supplementary_microscopy**). A cross section through the shell in direction of maximum growth
(**Figure 3A**) shows a layered shell structure with laterally continuous growth increments similar to
those in modern ostreids (e.g. Carriker et al., 1980b; Surge and Lohmann, 2008; MacDonald et al.,
2009; Ullmann et al., 2013). Growth increments are characterized by an alternation of dense,
foliated calcite layers with lighter coloured, more porous, vesicular ("chalky") calcite layers that are
characteristic for the family Gryphaeidae (Linnaeus, 1758; Carriker et al., 1980b; Bieler et al., 2004;
Surge and Lohmann, 2008). The porosity of these vesicular layers is visualized in microscopic images
(**Figure 3D-F**). The hinge of the shell is mostly devoid of this vesicular microstructure, but instead
consists of a close packing of foliated calcite layers (**Figure 3A** and **Figure 3H**). However, in parts of
the hinge small layers of vesicular calcite are also visible between the foliated layers (**Figure 3H**). In
places where these vesicular layers are interlocked between foliated layers, the transition between
the two microstructures is gradual. Further away from the shell hinge, the transitions between
foliated calcite and vesicular calcite are sharp and individual layers of foliated and chalky calcite can
be very thin (<30 µm; **Figure 3E-G**). Pores in the vesicular calcite are heterogeneous in size and shape
and can be up to 200 µm wide. While the shell structure is in general very well preserved (**Figure 3D-
H**), it is disturbed in some areas by patches of different texture, or holes that have been previously
ascribed to boring by polychaete worms (Brezina et al., 2014).

5.1.2 Porosity

Micro-CT images of specimen M4 further illustrate the distribution of porosity in the shell (**Figure 4**).
Porosity analysis based on micro-CT scanning confirms the microscopic observations of porous
vesicular calcite and denser foliated calcite layers in the shells. Quantitative analyses of porosity
through the shell (porosity logs) on the high-resolution CT scan of a small part of the shell (**Figure 4B**)
shows that the distribution of porosity strictly relates to growth layering of the shell. The porosity log
perpendicular to the layers (**Figure 4E**) shows that porosity is almost absent in the foliated calcite
layers and reaches up to 65% of the shell volume in the most porous vesicular layers. Total shell CT
scan results reveal that the average porosity in the shell is 21%.

5.1.3 Chemical heterogeneity and cathodoluminescence

Heterogeneity in the *P. vesicularis* shell is also evidenced by the distribution of iron (Fe) and
manganese (Mn) in the shell, as illustrated by µXRF mapping (**Figure 3B-C**). The maps show that the
vesicular layers are characterized by higher concentrations of Fe and Mn than the dense foliated
calcite layers. Parts of the shell that were perforated by bore holes have especially high
concentrations of Fe and Mn, and these holes are surrounded by a corona of elevated Fe and Mn

concentrations (**Figure 3I-L**). A close-up of a shell hinge (**Figure 3B and C**) confirms that it consists almost entirely of dense foliated calcite with low Fe and Mn concentrations. It also shows occasional thin layers of vesicular calcite with higher Mn concentrations between foliated calcite layers in the shell hinge (**Figure 3B**). The same close-up also illustrates that, due to the spot size of 25 μm, the method is not able to resolve variations in the concentration of Fe and Mn on the scale of fine (<30 μm) laminations in the shell hinge. A composite of cathodoluminescence microscopy images of the same area (insert in **Figure 3A**) complements μXRF mapping by showing in more detail that the foliated calcite of the shell hinge is characterized by microscopic growth increments that show a dull luminescence. At the same time, the vesicular calcite microstructure shows bright luminescence (**Figure 3A**, **supplementary data 3**). Only the largest increments can be distinguished on the μXRF map, while thin alternations between microstructures are generally too small for the 25 μm XRF spot size to detect. In calcite, Mn^{2+} is the main luminescence activator causing emission of yellow to orange light (~620 nm; Machel and Burton, 1991) of which the intensity is positively correlated with the Mn concentration (de Lartaud et al., 2010a; Habermann, 2002; Langlet et al., 2006; de Winter and Claeys, 2016). Indeed, brighter layers in the CL image correspond to higher Mn values in the XRF map. An enlarged version of the CL composite shown in **Figure 3** as well as CL-images of other parts of the shells are given in **supplementary data 3** and XRF Mn and Fe maps of all shells are given in **supplementary data 2**.

5.2 Trace element profiles

Raw results of XRF line scans through all *P. vesicularis* shells featuring in this study are given in **supplementary data 4**. Quantitative XRF line scans through the hings yield records of [Ca], [Si], S/Ca, Zn/Ca, Sr/Ca, Mg/Ca, [Mn] and [Fe] in growth direction through the dense hinge area of the shells (**Figure 5**). All measured XRF data are directly represented in **Figure 5**, only the Mg/Ca record is plotted with a three point running average. This smoothing is necessary because the Kα-energy in which Mg fluoresces X-rays is low, causing measurements and quantification of Mg to be more susceptible to small-scale changes in the sample matrix along the XRF scan, which can be smoothed out by a moving average (see de Winter and Claeys, 2016; de Winter et al., 2017b). Concentrations of calcium (Ca) and silicon (Si) in all shell records generally remain above 38 mass% and below 0.5 mass%, respectively. In three of the four specimens (M0, M4 and M6), absolute concentrations of Fe and Mn rarely exceed 800 μg/g (**Figure 5**). The iron record of specimen M11 shows maxima often exceeding 2000 μg/g. Fe concentrations in M6 are also elevated in comparison with M0 and M4, leading to the suggestion that there might be a link between the presence of bore holes (observed in M6 and M11) and elevated Fe-concentrations. A cross plot in **Figure 6A** shows that the concentrations of Fe and Mn are weakly correlated in XRF line scan measurements. Furthermore, samples with elevated concentrations of Mn generally have lower Sr concentrations, especially when Mn concentrations exceed 800 μg/g (**Figure 6B**). Both are a sign of diagenetic alteration because Mn and Fe have been shown to be preferentially enriched in recrystallized shell carbonates, while Sr is preferentially removed during the recrystallization process (Brand and Veizer, 1980; Al-Aasm and Veizer, 1986a). Trace element profiles through the four *P. vesicularis* specimens show that there is good agreement between shells both in terms of absolute concentration of magnesium (Mg), strontium (Sr), zinc (Zn) and sulphur (S) and their internal variation. Records of ratios of Mg/Ca, Sr/Ca, Zn/Ca and S/Ca show quasi-cyclic oscillations. In records of Mg/Ca and Sr/Ca, these oscillations appear sinusoidal, while records of Zn/Ca and S/Ca are characterized by short-lived increases relative to a baseline value. Trace element ratios generally oscillate around a stable baseline value, though in some cases (e.g. Sr/Ca and Mg/Ca in M11) there is a slight evolution of this baseline value in the direction of growth.

5.3 Stable isotope analysis

407 **5.3.1 Stable isotope records**

408 Records of $\delta^{18}O$ and $\delta^{13}C$ are plotted together with trace element ratios in **Figure 5**. As in trace
409 element records, absolute values as well as internal variation of stable isotope records show good
410 agreement between shells. Values in the $\delta^{18}O$ record oscillate around a baseline value of -1.5‰. The
411 $\delta^{13}C$ baseline values are more variable, possibly showing a late ontogenetic trend in M6 and M11,
412 but remaining stable at 2‰ in the other specimens. Stable oxygen and carbon isotope records seem
413 to show quasi-periodic variations around these baseline values, with amplitudes of about 1‰ and
414 0.5‰ respectively (**Figure 5**). Stable oxygen isotope ratios remain between -2.5‰ and -0.5‰ for the
415 majority of the records, only dropping below -3‰ in a few measurements in M4, the central part of
416 the M6 record, and a few measurements in the youngest part of the M0 record. Similarly, $\delta^{13}C$ ratios
417 in all shells remain between 1.5‰ and 3.5‰, except for the latter cases. Cross plots between
418 isotope ratios show that samples with exceptionally low $\delta^{18}O$ values (<-3‰) often also exhibit
419 decreased $\delta^{13}C$ values (<1.5‰; **Figure 6D**). This relationship between $\delta^{18}O$ and $\delta^{13}C$, which is
420 significant in shells M4, M6 and M11 but not in M0, is often interpreted as a sign of diagenetic
421 alteration (Al-Aasm and Veizer, 1986b; Banner and Hanson, 1990). Therefore, the absence of this
422 relationship in M0 in contrast to the other shells shows that the stable isotope profile from the hinge
423 of shell M0 is least affected by diagenetic alteration. The fact that $\delta^{18}O$ and $\delta^{13}C$ values are generally
424 lower in samples with elevated concentrations of Mn and Fe (**Figure 6A and 6C**) supports the
425 hypothesis that these parts of the shell are affected by diagenesis.

426 **5.3.2 Clumped isotope analysis**

427 Clumped isotope analyses of ventral margin calcite from three *P. vesicularis* shells from the same
428 palaeoenvironment (M5, M8 and M10; see **Figure 1** and section 4.1) yielded Δ_{47} values of 0.699 to
429 0.707‰, equivalent to a temperature range of 21-25°C using the high temperature composite
430 calibration of Defliese et al. (2015; see **Table 1**). Both reconstructed temperatures and $\delta^{18}O_{seawater}$
431 values varied significantly between these samples, with $\delta^{18}O_{seawater}$ ranging from -0.6‰ in M10 to -
432 2.2‰ and -5.9‰ in M5 and M8 respectively, likely indicating the influence of altered calcite
433 material. This is supported by shell $\delta^{18}O$ values, which contain very low values (-4‰ to -7‰VPDB in
434 M5 and M8) well outside of the range of samples micromilled from the well-preserved hinge
435 carbonate (**Figure 5**). The same samples (M5 and M8) also show relatively decreased $\delta^{13}C$ values
436 (<1‰), indicating that these decreased stable isotope ratios are likely indicative of diagenetic
437 alteration. In comparison, samples of the dense hinge calcite from M4, M5, M8 and M11, yielded Δ_{47}
438 values of 0.725 to 0.746‰, corresponding to much cooler temperatures of 9-15°C and $\delta^{18}O_{seawater}$
439 values ranging from -1.8‰ to -3.4‰ (-2.8‰ on average). Shell $\delta^{13}C$ and $\delta^{18}O$ values from bulk
440 samples of hinge carbonate resemble values measured in the high-resolution transects, showing that
441 carbonate in the shell hinges is well preserved.

442

443 **6. Discussion**

444 **6.1 Shell preservation**

445 **6.1.1 Visualization of diagenesis**

446 Results of CT scanning and microscopy show that, while calcite in the vesicular microstructure was
447 affected by recrystallization, the original porosity in *P. vesicularis* shells has been preserved almost
448 completely, and the filling of pores by calcite cementation is relatively uncommon (see **Figure 3D-E**).

449   Microscopic images of the foliated calcite microstructure (e.g. **Figure 3F-G**) and comparison with
450   modern oyster studies further show that the elongated crystal microstructure characteristic of
451   pristine foliated shell calcite has not been compromised by diagenesis (Ullmann et al., 2010).
452   Elevated concentrations of Fe and Mn in the shells can be used as an indicator for recrystallization,
453   since these elements are incorporated in secondary calcite from reducing pore waters in the
454   sediment surrounding the shell during burial (Al-Aasm and Veizer, 1986a). This makes µXRF maps of
455   Fe and Mn concentrations excellent tools for the assessment of primary calcite preservation. The
456   maps in **Figure 3B and C** shows that such recrystallization is predominantly observed in the vesicular
457   calcite and that Fe and Mn concentrations in foliated calcite layers are low. Coronas of elevated Fe
458   and Mn concentrations around bore holes confirm that Mn and Fe were leached into the shell
459   through these holes when pore fluid infiltrated the shell and were distributed through the porous
460   vesicular calcite layers. The layered macrostructure of ostreid shells facilitated this penetration of
461   pore fluids. The fact that shells M6 and M11, containing the most bore holes (see **Figure 2**), have the
462   highest Mn and Fe values (**Figure 5**) supports this hypothesis. CL microscopy images showing
463   minimal dull luminescence in the foliated calcite and bright luminescence in vesicular calcite confirm
464   leaching of Mn and Fe into the shells (Barbin, 2000). Brightly luminescing laminae between foliated
465   calcite layers in the shell hinge are associated with peaks in Mn and Fe observed in the µXRF profiles
466   of M11 (**Figure 5**). Comparison between the CL composite and the µXRF map shows that, while µXRF
467   mapping does pick up large scale diagenetic features in the shell, it fails to reveal most of the small
468   layers intercalated between foliated calcite layers in the shell hinge because they are smaller than
469   the spot size of the µXRF scanner (25 µm). This illustrates that µXRF mapping is a useful tool for
470   screening diagenetic overprint, but fails to pick up the fine details that are visualized by CL-
471   microscopy. Similarly, Mn and Fe profiles in µXRF line scanning will miss or average out the small
472   layers of vesicular calcite present in some parts of the shell hinges of *P. vesicularis* and CL-
473   microscopy remains a necessary tool for thorough screening for diagenesis.

474   **6.1.2 Diagenesis in trace element profiles**

475   Quantitative XRF line scans through the hinges of *P. vesicularis* show that absolute concentrations of
476   Fe and Mn rarely exceed 800 µg/g in all shells except for M11 (**Figure 5**). Mn concentrations
477   measured in the hinges are higher than is considered typical for well-preserved bivalve calcite and
478   often exceed the diagenesis threshold of 300 µg/g proposed by Steuber (1999). However, high
479   concentrations of Sr (>700 µg/g) and Mg (>1000 µg/g), comparatively low Fe concentrations and the
480   observation of non-luminescent, well-preserved foliated calcite crystals (**Figure 3**) suggest
481   preservation of the original trace element signature (Veizer, 1983; Al-Aasm and Veizer, 1986a;
482   Steuber, 1999). The fact that parts of shells with more depleted stable isotope ratios and lower Sr
483   concentrations generally coincide with peaks in Fe and Mn exceeding 800 µg/g shows that these
484   results likely signify areas where recrystallization has occurred (see also **Figure 5 and 6A-C**). We
485   therefore propose 800 µg/g as a tentative maximum threshold for Mn and Fe concentrations for the
486   preservation of pristine calcite in shells of *P. vesicularis* in this setting, and consider samples
487   exceeding this threshold in concentration for either Mn or Fe as diagenetically altered. Evidence of
488   such alteration is most common in shells M6 and M11. Except for a few measurements in shells M6
489   and M11, low Si concentrations and high Ca concentrations (**Figure 5**) indicate limited incorporation
490   of detrital material into the hinge of the shell (see de Winter and Claeys, 2017; de Winter et al.,
491   2017a). Indeed, bore holes filled by detrital material are almost exclusively observed away from the
492   shell hinge and did not significantly influence XRF records (**Figure 2 and 3**). From this it follows that
493   the majority of post-mortem alteration of the shells occurred through the process of chemical
494   alteration (e.g. recrystallization) rather than physical processes (e.g. predatory burrowing). As
495   described above (see 5.1.1), the role of bore holes in the shells (especially M6 and M11) in the

496 diagenetic process was predominantly to provide entries through which pore waters could enter to
497 cause recrystallization. Bore holes elsewhere in the shells may lead to migration of fluids through the
498 shell, ultimately resulting in elevated concentrations throughout the shell.

499 **6.1.3 Diagenesis in stable isotope records**

500 The majority of the stable isotope ratios measured the shell records are in agreement with those of
501 well-preserved Low Magnesium Calcite of fossil (Steuber, 1996; 1999; Tripati et al., 2001) and
502 modern marine mollusc shells (Klein et al., 1996a;b; Goodwin et al., 2001; Lécuyer et al., 2004). $\delta^{18}O$
503 and $\delta^{13}C$ values below -4‰ and 1‰ respectively (a drop of 2-3‰ for $\delta^{18}O$ and 1-2‰ for $\delta^{13}C$) in the
504 central part of the M6 shell hinge record are an exception to this and likely represent incorporation
505 of diagenetically altered vesicular calcite into micromilled IRMS samples. The scan image of M6
506 (**Figure 2**) shows that an extension of vesicular calcite into the hinge region resulted in the sampling
507 of vesicular calcite in the stable isotope and trace element records. Similarly, the stable isotope
508 record of specimen M4 was affected by lobes of vesicular calcite extending close to the hinge line. A
509 depletion of both $\delta^{18}O$ and $\delta^{13}C$ could potentially also be explained by an input of freshwater into
510 the basin (Gillikin et al., 2006), but the scale of the isotopic shift and the fact that they coincide with
511 increases in vesicular calcite shows that diagenetic alteration is a more likely explanation. Low $\delta^{18}O$
512 values in vesicular calcite samples could also suggest that this vesicular calcite was initially
513 precipitated in disequilibrium with respect to ambient sea water (Grossman and Ku, 1986; Woo et
514 al., 1993; Steuber, 1999). The latter could be in agreement with the hypothesis that vesicular
515 microstructures in oyster shells are formed by microbes instead of by the bivalve itself (Vermeij,
516 2014). However, microscopic images of the vesicular microstructure reveal blocky calcite crystals in
517 some areas (**Figure 3E-F**), which suggest recrystallization (e.g. Folk and Land, 1975; Schlager and
518 James, 1978). Indeed, the offset in stable isotope ratios of vesicular calcite compared to foliated
519 calcite is not found in modern oyster shells (Surge and Lohmann, 2008; Ullmann et al., 2010).
520 Elevated Mn and Fe concentrations found in XRF mapping (**Figure 3B-C**), and the notion that similar
521 chalky or vesicular phases in modern oyster shells are less crystalline and grow faster (Chinzei and
522 Seilacher, 1993; Ullmann et al., 2010), further attest to the fact that vesicular calcite in *P. vesicularis*
523 (and likely in other fossil members of the Gryphaeidae) is more prone to diagenetic alteration than
524 its foliated counterpart, and therefore provides no suitable record of palaeoclimatic information.

525 This conclusion is also supported by the clumped isotope analysis results. Bulk samples from the
526 ventral margin of the shell (containing more vesicular calcite, see **Figure 2 and 3**) contain lower
527 stable isotope ratios and higher reconstructed temperatures than samples from the dense shell
528 hinge (**Table 1**; **Figure 7**). Elevated temperatures in altered samples likely reflect recrystallization of
529 shell material from slightly warmer pore fluids after burial. Comparison of Δ_{47} with $\delta^{18}O$ and $\delta^{13}C$
530 measurements (**Figure 7**) clearly show how the sensitivity of clumped isotope analysis can be used to
531 demonstrate the effect of calcite recrystallization within *P. vesicularis*. Sequential sampling for Δ_{47}
532 measurements in bivalve calcite therefore may provide a useful tool to trace intra-shell variability in
533 preservation and calcification temperature. Temperatures from diagenetic samples (average = 23°C)
534 are relatively low compared to typical pore fluid temperatures measured from diagenetic calcite in
535 other studies (30-120°C; Huntington et al., 2011; Loyd et al., 2012; Dale et al., 2014), and do not
536 deviate much from those of pristine samples (23°C vs. 11°C; **Table 1**). This suggests that burial was
537 shallow and recrystallization not extensive. The shallow burial history is also demonstrated by the
538 preservation of organic biomarkers in the Bajada de Jagüel section (Woelders et al., 2017). With a
539 maximum burial temperature of 25°C during recrystallization, the burial depth of the late
540 Maastrichtian strata in the Neuquèn Basin is likely to be very shallow and at the very maximum no
541 more than 500 meters (Klein et al., 1999; Dale et al., 2014).

6.1.4 Implications for sampling strategy

Contrary to what may be expected, the incorporation of vesicular calcite into the stable isotope samples of M6 (**Figure 2 and 5**) is not always reflected by elevated Mn and Fe concentrations in the μXRF line scans. This could suggest that trace element signatures in vesicular calcite close to the hinge are less affected by the leaching of reducing pore waters than in the rest of the shell. Alternatively, it is likely that the 2 mm wide sampling track for stable isotope measurements contains more vesicular calcite than the 25 μm wide XRF line. This shows that the wide sampling track needed to sample for stable isotope analysis at high spatial resolution (100 μm in the direction of growth) increases the chance of incorporating vesicular calcite, particularly in samples further away from the hinge line and in shells where vesicular calcite layers penetrate close to the hinge line (e.g. M4 and M11, see **Figure 2, Figure 3 and Figure 6D**). This illustrates a disadvantage of the abrasion-style microdrilling method applied in this study for spatially heterogeneous bivalves, and shows that thorough screening for diagenesis by CL-microscopy and μXRF mapping is essential to correctly interpret the stable isotope results.

Summarizing, shells M6 and M11 are characterized by elevated Fe and Mn concentrations in the shell hinge line, signifying that these specimens contain larger amounts of recrystallized vesicular calcite in their shell hinge. Specimen M4 shows lower Fe and Mn concentrations in the shell hinge, but low stable isotope ratios show that several microdrilled samples contain diagenetically altered vesicular calcite. Stable carbon and oxygen isotope ratios in shells M4, M6 and M11 all show a significant positive relationship, while such a relationship is absent in M0. As a result, of the 4 specimens investigated, specimen M0 is considered to represent the best preserved specimen, most likely providing the most reliable results in terms of palaeoenvironmental reconstruction. Coloured vertical bars in **Figure 5** illustrate parts of the shell records that were considered altered based on one or more of the criteria described above: 1) Bright luminescence in CL-microscopy. 2) Elevated (>800 μg/g) Fe and/or Mn concentrations. 3) Elevated Si (>0.5 mass%) and reduced Ca (<38 mass%) concentrations. 4) Decreased stable isotope ratios ($\delta^{18}O < -3‰$ and $\delta^{13}C < 1.5‰$).

6.2 Periodic variations

6.2.1 Shell chronology

While earlier studies have been successful in determining the chronology of geochemical records from Quaternary fossil bivalves (e.g. Scourse et al., 2006; Marali and Schöne, 2014), attempts at palaeoseasonality reconstructions based on more ancient shells have shown that this is not straightforward (Dettmann and Lohmann, 1993; Bougeois et al., 2014; de Winter and Claeys, 2016; de Winter et al., 2017a). In this study, quasi-periodic variations in stable oxygen isotopes, Sr/Ca ratios and Mg/Ca ratios seem to represent seasonal cycles in shell growth (**Figure 5**), but on closer inspection it is difficult to find a consistent phase relationships between these records through all four shells. The best-preserved record (M0) was tentatively subdivided into annual cycles based on Sr/Ca and $\delta^{18}O$ seasonality. **Figure 8** shows a stack of the trace element records created based on these subdivisions. Similar year stacks of the other three shells yielded different phase relationships between proxies (**supplementary data 5**). These differences are likely explained by the incorporation of diagenetically altered vesicular calcite in some of the microdrilled samples, resulting in significantly lighter $\delta^{18}O$ and $\delta^{13}C$ values. The record of shell M4 (**Figure 5**) clearly illustrates how diagenesis can preferentially influence one season over the other and result in a change of the phase relationship between proxies in the shell. Since incorporation of lobes of vesicular calcite into the shell hinge seems to be paced to the seasonal cycle, it is difficult to disentangle patterns of diagenetic alteration from seasonal patterns. Such preferential incorporation of vesicular calcite into

587 the hinge during one season can occur when the bivalve experiences more physiological stress in
588 that season (Müller, 1970). Indeed, even when diagenetically altered parts of these records
589 (according to the threshold of 800 μg/g for Fe and Mn and -3‰ for $\delta^{18}O$) are excluded, seasonal
590 patterns in year stacks of shells M4, M6 and M11 do not fully agree with those in the better
591 preserved M0 shell, showing that poorer preservation prevents the establishment of a reliable
592 chronology for these shells. That said, records from shells M4, M6 and M11 should not be dismissed,
593 as variation in the geochemical proxies measured in pristine parts of these shells could still yield
594 valuable information about the extent of seasonality during their growth, even though phase
595 relationships are blurred by diagenetic overprinting. Moreover, since the exact stratigraphic level of
596 the shells is not fully constrained, small differences in expression of the proxies due to changes in
597 environment between their lifetimes cannot be fully excluded. The fact that microdrill and μXRF
598 tracks in these shells were not exactly the same further complicates the establishment of consistent
599 phase relationships between geochemical records in the shells. For example, stable isotope samples
600 were more severely laterally averaged (2 mm wide track compared to 25 μm wide μXRF transect),
601 and had to be rescaled to the length of XRF records before being plotted in **Figure 5** (see section
602 4.5).

603 **6.2.2 Phase relationships**

604 The year stack of the well-preserved specimen M0 (**Figure 8**) shows that the $\delta^{18}O$, $\delta^{13}C$ and Sr/Ca
605 records exhibit a sinusoidal pattern with one peak per year. In contrast, records of Zn/Ca, S/Ca and
606 Mg/Ca show two peaks in each year. Comparing these observations with the records in **Figure 5**
607 shows that the same seems to be true for the pristine parts of the other three shells. In addition, the
608 M0 year stack shows that maxima in $\delta^{13}C$ ratios coincide with minima in Sr/Ca and Zn/Ca and that
609 minima in $\delta^{13}C$ ratios shortly follow minima in $\delta^{18}O$. Zn/Ca and S/Ca records show an antiphase
610 relationship, and the Mg/Ca record has one minimum that coincides with a minimum in $\delta^{18}O$ ratios
611 and another offset by half a cycle. Yet, since only one of the shells measured in this study (M0)
612 showed good enough preservation for a discussion of phase relationships between records, care
613 must be taken in extrapolating the conclusions drawn from the year stack of this single shell.

614 **6.3 Interpreting geochemical records in *Pycnodonte vesicularis***

615 6.3.1 Comparison with other taxa

616 Carbon isotope values found in this study are higher than in oysters living in modern coastal
617 temperate environments (Surge et al., 2001; Ullmann et al., 2010), but more similar to oysters living
618 in warmer, high-salinity or tropical settings (Klein et al., 1996a; Surge and Lohmann, 2008; Titschack
619 et al., 2010). Oxygen isotope ratios are generally lower than modern coastal mid latitude bivalves
620 (Klein et al., 1996b; Ullmann et al., 2010) and in better agreement with warmer, low latitude studies
621 (Lécuyer et al., 2004) and other Cretaceous bivalves (Steuber, 1999). This is in agreement with
622 reconstructions of $\delta^{18}O$ ratios in Late Cretaceous oceans that were ~1‰ lower compared to the
623 present-day ocean due to the absence of extensive polar ice sheets (e.g. Hay, 2008), and also with
624 the warmer palaeoenvironmental setting inferred for the Late Cretaceous of Neuquén Basin, based
625 on TEX_{86}-palaeothermometry (Woelders et al., 2017). However, the clumped isotope thermometry
626 results of this study suggests rather cooler temperatures. In order to properly interpret geochemical
627 records from *P. vesicularis*, it is important to compare the results of this study with those from
628 closely related bivalves. Although the genus *Pycnodonte* has no living members, two sister taxa in
629 the subfamily Pycnodonteinae (Stenzel, 1956) contain extant members: *Hyotissa* and
630 *Neopycnodonte* (Stenzel, 1971).

6.3.2 *Hyotissa hyotis* (Linnaeus, 1758)

The microstructure of *Hyotissa hyotis* is similar to that of *P. vesicularis*, with porous vesicular phases alternating with dense foliated calcite layers. A specimen of *Hyotissa hyotis* in the northern Red Sea was subject to a stable isotope study by Titschack et al. (2010). In contradiction to findings by Nestler (1965), but similar to *H. hyotis* (Titschack et al., 2010) and modern oysters like *Crassostrea virginica* (Surge and Lohmann, 2008) and *Crassostrea gigas* (Ullmann et al., 2010), seasonal variations in $\delta^{18}O$ and $\delta^{13}C$ in *P. vesicularis* were found to be independent of shell microstructure (foliated vs vesicular calcite). This shows that the isotopically light signal of the vesicular calcite in the records of M4, M6 and M11 was caused by recrystallization, disturbing the seasonality signal in their stable isotope records, hampering the interpretation of shell chronology (see 6.2.1). Stable carbon isotope ratios in *P. vesicularis* resemble those measured in *H. hyotis* in terms of absolute values and seasonal amplitude. In principle, the $\delta^{13}C$ of shell carbonate is controlled by the $\delta^{13}C$ value of the dissolved inorganic carbon (DIC) of the organism's extrapallial fluid (EPF), from which the shell is precipitated (Kirby, 2000). In marine bivalves, the $\delta^{13}C$ of the EPF is controlled by the $\delta^{13}C$ of ambient seawater, the carbonate ion pump, pH, food availability, growth, valve gape/closure intervals, and seasonal changes in metabolic rate (Romanek et al., 1992; McConnaughey et al., 1997; Kirby et al., 1998; Owen et al., 2002; Geist et al., 2005; McConnaughey and Gillikin, 2008; Lartaud et al., 2010b). The variation in all these processes complicates practical interpretation of the $\delta^{13}C$ signal (Lorrain et al., 2004; Omata et al., 2005). In *H. hyotis*, $\delta^{13}C_{shell}$ is controlled by bivalve respiration, which increases during periods of enhanced planktonic food supply (Titschack et al., 2010). A shifted phase relationship between $\delta^{18}O$ and $\delta^{13}C$ in *H. hyotis*, similar to the phase shift observed in **Figure 8**, is attributed to phase-shifted cycles in sea surface temperature and productivity. Comparison with modern *H. hyotis* therefore suggests that annual lows in $\delta^{13}C$ values in *P. vesicularis* also indicate periods of increased food supply, such as plankton blooms.

6.3.3 *Neopycnodonte zibrowii* (Videt, 2004)

While the large bivalve *Neopycnodonte zibrowii* shows similar alternations in vesicular and foliated calcite as *P. vesicularis*, it is deep dwelling (450–500m), in contrast with the shallow marine taxa *P. vesicularis* and *H. hyotis*, and has a much longer lifespan. A specimen of *N. zibrowii* (Videt, 2004) was subject of a detailed multi-proxy analysis in Wisshak et al. (2009). The shell of *N. zibrowii* is characterized by much higher Mg/Ca and S/Ca and lower Sr/Ca ratios than that of *P. vesicularis*. Coincidence of peaks in Mg/Ca and S/Ca coinciding with minima in Ca and Sr concentrations in *N. zibrowii* can be interpreted as evidence for strong vital effects controlling trace element concentrations rather than external forcing (e.g. by temperature; Lorens and Bender, 1980; Rosenberg and Hughes, 1991). Such relationships between Mg/Ca, S/Ca and Sr/Ca are not observed in *P. vesicularis* (**Figure 5**, **Figure 6** and **Figure 7**). Contrary to other modern oyster studies (Surge and Lohmann, 2008; Titschack et al., 2010; Ullmann et al., 2010), Wisshak et al. (2009) report an isotopic offset between vesicular and foliated calcite. However, $\delta^{18}O$ values in vesicular calcite of *N. zibrowii* are higher than in its foliated calcite, opposite to *P. vesicularis* (**Figure 5**). Similarly, a strong negative ontogenetic trend in $\delta^{13}C$, which is absent in *P. vesicularis* and most extant oysters (**Figure 5**; Surge et al., 2001; Surge and Lohmann, 2008; Ullmann et al., 2010), was observed in the juvenile part of *N. zibrowii* records. While such a juvenile trend in $\delta^{13}C$ is uncommon, trends later in life have been reported for other taxa and are thought to be caused by increasing utilisation of isotopically light metabolic carbon for shell calcification (Lorrain et al., 2004; Gillikin et al., 2007). The vast difference in geochemical records between these closely related bivalve taxa (*Neopycnodonte* and *Pycnodonte*) shows that environmental setting and mode of life (growth and metabolic rates) play a large role in governing vital effects. Geochemical records in the shell of the deep-dwelling *N. zibrowii* are clearly

15

677   strongly controlled by vital effects, and both shell chemistry and environmental setting of *P.*
678   *vesicularis* show much closer resemblance to *H. hyotis* and marine *Crassostrea gigas* (Surge and
679   Lohmann, 2008; Ullmann et al., 2010) than to those of *N. zibrowii*.

680   6.3.4 Timing of shell deposition and seasonality

681   The $\delta^{18}O$ records of *H. hyotis* are strongly correlated with both Sea Surface Temperature (SST) and
682   Sea Surface Salinity (SSS; TItschak et al., 2010). The fact that $\delta^{18}O$ values in shells of *H. hyotis* are
683   higher than in *P. vesicularis* is likely because the former grew in an environment characterized by net
684   evaporative conditions (Safaga Bay, Egypt). As a result, salinity and $\delta^{18}O_{seawater}$ (+2.17‰) were higher
685   than in the Neuquén Basin (-2.8‰). Indeed, Woelders et al. (2017) argued that the late
686   Maastrichtian environmental setting of Bajada de Jaguël was influenced by freshwater input, based
687   on organic-walled dinoflagellate cysts, benthic foraminifera and organic biomarker proxies. Crucially,
688   the Neuquèn Basin is interpreted to have been characterized by a strong summer precipitation
689   maximum, suggesting that the lowest $\delta^{18}O$ values in our yearstack correspond to highest summer
690   temperatures and lowest salinities (December - January). The $\delta^{18}O$ curve in our yearstack is strongly
691   asymmetrical, the $\delta^{18}O$ minimum peak being truncated. Such a truncation potentially reflects slower
692   growth or a growth stop in the summer season. We propose that, while in modern oysters growth is
693   often limited by low water temperature in the winter season (e.g. Ullmann et al., 2010, 2013),
694   increased temperatures and low salinities in the summer season of the Late Cretaceous Neuquèn
695   Basin have limited growth of *P. vesicularis*. The effect of a similarly co-varying SSS and SST on bivalve
696     $\delta^{18}O$ and $\delta^{13}C$ has been studied in *Crassostrea virginica* growing under changing salinity conditions
697   (Surge et al., 2001). However, in contrast to estuarine *C. virginica* studied by Surge et al. (2001),
698   where both stable isotope records are in phase, the best preserved specimen in our study (M0)
699   presents a shifted phase relationship between $\delta^{18}O$ and $\delta^{13}C$. Counterintuitively, following the
700   rationale that the lowest $\delta^{18}O$ values in our record reflect to the summer precipitation maximum,
701   the annual drop in $\delta^{13}C$, corresponding to months with the highest planktonic food supply, would
702   occur shortly after growth-limiting summer conditions (February - March).

703   6.3.5 Palaeoproductivity

704   The coinciding of minima in Zn/Ca with maxima in S/Ca and minima in $\delta^{18}O$ in the well preserved M0
705   specimen (**Figure 5 and 6**) is in agreement with the interpretation of the seasonal palaeoproductivity
706   cycle. Zn concentrations in bivalve shells drop during productivity blooms, which occur late in the
707   summer season (February-March; Calvert and Pedersen, 1993; Jackson et al., 1993; Guo et al., 1997,
708   de Winter et al., 2017a). Spring blooms affected the amount of bio-available Zn in the surface ocean
709   and forced a drop in Zn/Ca ratios in the shells of *P. vesicularis* (Guo et al., 2002). This explains why
710   minima in Zn/Ca coincide with the lowest $\delta^{18}O$ values, which occur in summer and precede the
711   minima in $\delta^{13}C$ which reflect a seasonality in productivity as in *H. hyotis*. Increased fresh water input
712   into the basin during summer, which caused the warm, low salinity conditions observed in the $\delta^{18}O$
713   records, could have provided the nutrients that initiated this productivity bloom.

714   6.3.6 Physiological effects

715   The observed anti-correlation between $\delta^{18}O$ and S/Ca in M0 suggests that S/Ca in *P. vesicularis*
716   responded to seasonal changes in food availability, growth or respiration rate. In other groups of
717   bivalves S/Ca ratios were shown to reflect periods of high metabolic rate and slow shell growth (e.g.
718   Rosenberg and Hughes, 1991). Similarly, environmental stress, such as temperature or salinity
719   extremes, have been linked to a decrease in growth rate an increase in the incorporation of sulphur
720   into the organic matrix of the bivalve shell (Lorens and Bender, 1980). Therefore, a peak in S/Ca

721 during the summer season, when growth rate presumably decreased, is in agreement with this
722 explanation. The observation that the amplitude of S/Ca variations in the record of M6 increases in
723 the part of the shell where vesicular calcite penetrates the shell hinge (**Figure 5**) supports the
724 hypothesis that these disturbances of the shell hinge indicate periods of physiological stress
725 experienced by the bivalve (Müller, 1970). The anti-phase relationship between S/Ca with Zn/Ca and
726 δ^{13}C minima show that the productivity blooms discussed above affected growth and metabolic rate
727 in *P. vesicularis*.

728 Similarly, a decrease in Sr/Ca ratios synchronous with the peak in δ^{13}C suggests that both proxies are
729 controlled by physiology. The interpretation that Sr/Ca ratios are lower during the low-salinity
730 summer season in which growth was slower is in agreement with relationships between Sr/Ca and
731 growth rate found in modern bivalves (e.g. Gillikin et al., 2005a; Lorrain et al., 2005). However, if
732 Sr/Ca is indeed controlled by growth rate, one would expect to see an ontogenetic drift of Sr/Ca
733 towards lower ratios as the shell extends more slowly as the animal ages. Yet, this effect is not
734 clearly expressed by our specimens, indicating that either *P. vesicularis* did not exhibit such a
735 decreasing trend in growth rate with age or that the relationship between Sr/Ca and growth rate is
736 not straightforward.

737 **6.4 Temperature proxies**

738 An overview of all temperature proxies used in this study is plotted in **Figure 9**, illustrating the
739 complexity of combining these different proxies in *P. vesicularis* to reconstruct palaeoseasonality.
740 Combination of the $\delta^{18}O_{sw}$ values reconstructed using clumped isotope analysis with the high-
741 resolution $\delta^{18}O$ records yields a sub-annual palaeotemperature reconstruction for all records.
742 However, the variations in these records may not reflect true sub-annual temperature variations,
743 especially since it is likely that salinity in the Neuquén Basin did not remain constant through the
744 year (see 6.3.4). Clumped isotope temperature reconstructions are similar to present-day average
745 annual surface water temperatures in the region (~10-15°C; Servicio Meteorológico Nacional, 2017),
746 while they are below model and proxy-based SST reconstructions for the Maastrichtian mid-latitudes
747 (20-25°C; e.g. Donnadieu et al., 2006; Brugger et al., 2017; O'Brien et al., 2017) and average air
748 temperatures inferred for the Maastrichtian Neuquén Basin based on the megathermal vegetation
749 (>24°; Barreda and Palazzesi, 2007; Palazzesi and Barreda, 2007; Barreda et al., 2012). The
750 systematically lower clumped isotope-based temperatures can partially be explained by the fact that
751 TEX$_{86}^{H}$ is calibrated to sea surface temperatures while *P. vesicularis* lived on the sea floor, at depths
752 of 50-75 m (Scasso et al., 2005). This means that, while TEX$_{86}^{H}$ reflects SSTs, the *P. vesicularis*
753 clumped isotope-based temperatures reflect the temperatures of the bottom waters, which must
754 have been slightly cooler than those at the sea surface. However, this difference is likely not enough
755 to explain the offset of ±15°C between clumped isotope and TEX$_{86}^{H}$ temperature reconstructions.
756 Over the past years, several studies have highlighted the complexity of shallow marine TEX$_{86}$ records
757 and have shown that temperature reconstructions by this method may be biased (e.g. Jia et al.,
758 2017). Similarly, in the compilation study of O'Brien et al. (2017), Cretaceous TEX$_{86}$-based sea surface
759 temperatures are systematically higher than planktic foraminiferal $\delta^{18}O$-based temperatures. In
760 some settings, TEX$_{86}$ is shown to be biased towards summer temperatures (Schouten et al., 2013). It
761 is possible that the same bias also applies to the Neuqúen basin TEX$_{86}^{H}$ reconstructions. On the other
762 hand, clumped isotope thermometry on *P. vesicularis* relies on bulk samples and yields mean value
763 of the entire growth season of the bivalve. Since growth in *P. vesicularis* seems to have slowed or
764 ceased during the spring and summer season (see 6.3.4 and 6.3.6), summer temperatures are likely
765 underrepresented in the clumped isotope reconstructions, biasing them towards lower
766 temperatures. It is therefore likely that the mean annual temperature in this setting lies in between

767   clumped isotope thermometry and TEX$_{86}^{H}$ estimates. Another source of bias for clumped isotope
768   thermometry on bulk samples is the incorporation of diagenetically altered vesicular calcite into the
769   shell hinge as a result of more stressful growth conditions (Müller, 1970; see 6.2.1). However, this
770   would have biased the reconstruction towards higher temperatures, while the opposite is observed.
771   In practice it will be difficult to avoid these lobes of vesicular calcite and small amounts are likely to
772   be included in clumped isotope samples, leading to higher palaeotemperature reconstructions.

773   While several temperature calibrations exist for Mg/Ca ratios in bivalves, the most likely candidates
774   for temperature reconstruction based on Mg/Ca of *P. vesicularis* are the calibrations based on other
775   ostreid bivalves. A good candidate would be the calibration by Surge and Lohmann (2008; based on
776   *Crassostrea virginica*). An alternative calibration by Mouchi et al. (2013) was based on juvenile
777   specimens of the pacific oyster *Crassostrea gigas* and is probably not suitable for application on
778   records from gerontic specimens. The Mg/Ca ratio of ocean water (Mg/Ca$_{ocean}$) has changed
779   drastically over geological timescales, and is thought to have been much lower in the late
780   Maastrichtian than in the present-day ocean (1-2 mol/mol compared to 5 mol/mol in the modern
781   ocean; Stanley and Hardie, 1998; Coggon et al., 2010). This difference most likely influenced Mg/Ca
782   ratios in calcifying organisms (Lear et al., 2015), and needs to be corrected for (de Winter et al.,
783   2017a) when applying the Mg/Ca thermometer. With this correction, the *C. virginica* temperature
784   calibration by Surge and Lohmann (2008; **Figure 9**) approach reconstructions based on the other
785   proxies in terms of temperature seasonality, yielding sea water temperatures of 20°C ± 10°C, slightly
786   higher than those observed in the $\delta^{18}O_{sw}$-corrected $\delta^{18}O$ record.

787   Since Mg/Ca ratios yield temperatures between clumped isotope and TEX$_{86}^{H}$ reconstructions, it is
788   tempting to assume that they more closely approximate mean annual temperatures than the other
789   proxies. However, while the seasonal bias caused by growth cessations in *P. vesicularis* should affect
790   Mg/Ca as much as $\delta^{18}O$, there are large differences (>10°C) between temperature reconstructions of
791   Mg/Ca and $\delta^{18}O$ in some parts of the records. Moreover, Mg/Ca ratios and $\delta^{18}O$ are anti-correlated
792   in parts of the well-preserved M0 record, suggesting that at least one of the proxies may largely be
793   controlled by a factor other than ambient temperature. Seasonal changes in salinity cannot account
794   for this difference between the proxies, since an unrealistic change in salinity would be required,
795   which is not consistent with earlier palaeoenvironmental reconstructions in the Neuquén Basin
796   (Prámparo et al. 1996; Prámparo and Papú 2006; Ravelo and Hillaire-Marcel, 2007; Woelders et al.,
797   2017). The shift between Mg/Ca and $\delta^{18}O$ records may also be a result of the relative scaling and
798   aligning of records measured using two different methods. Nevertheless, the uncertainties of Mg/Ca
799   temperature reconstructions in bivalves, together with the observed lack of temperature
800   dependence of Mg/Ca ratios in the closely related *N. zibrowii* shows that temperature
801   reconstructions based on Mg/Ca ratios in *Pycnodonte* oysters are probably not very robust.

802   Based on these observations, the best approach to reconstruct palaeotemperature seasonality from
803   *Pycnodonte* shells would be to microsample the foliated calcite of the shells for clumped isotope
804   analysis. This microsampling can be guided by records of conventional stable isotope ratios and trace
805   element concentrations to ensure the sampling of material from different seasons. Via this
806   approach, both seasonality in temperature and salinity can be reconstructed from *Pycnodonte* shells,
807   and the effects of salinity and temperature on $\delta^{18}O$ values can be disentangled.

808   **7. Conclusions and recommendations**

809   The multi-proxy approach applied in this work demonstrates the complexity of palaeoenvironmental
810   reconstruction on the seasonal scale. Based on this study, several recommendations can be made
811   for the use of *P. vesicularis* shells for palaeoseasonality and palaeoenvironment reconstruction.

812   Detailed analysis of shell structure and preservation shows that shells of *P. vesicularis*, like other
813   species of the Order Ostreoida, are characterized by two major micromorphologies of calcite, which
814   were referred to by Carriker et al. (1980b) as "chalky" and "foliated" calcite. In the case of *P.*
815   *vesicularis*, CT scanning shows that these "chalky" (vesicular) calcite layers are very porous (up to
816   65%) and permeable for pore fluids (**Figure 4**), making it prone to recrystallization (**Figure 3**). The
817   presence of bore holes, such as those made by polychaete worms, facilitates this penetration of
818   pore fluids. Its susceptibility to diagenesis renders the vesicular calcite of pycnodontein bivalves
819   poorly suitable for palaeoenvironmental reconstruction. Foliated calcite layers in the shell hinge of *P.*
820   *vesicularis* are less affected by diagenesis and seem to preserve primary calcite, making it suitable
821   for palaeoseasonality reconstructions. However, lobes of vesicular calcite can extend into the hinge
822   of the shells and complicate palaeoseasonality reconstructions based on stable and clumped isotope
823   measurements. Highly localized recrystallization and precipitation of secondary carbonates in
824   equilibrium with these reducing pore fluids increases the concentrations of Mn and Fe (see XRF
825   mapping and CL images in **Figure 3**) and lowers stable isotope ratios. Hence, micro-analytical
826   techniques such as cathodoluminescence microscopy, optical microscopy and µXRF mapping allow
827   these zones of recrystallization to be avoided.

828   Palaeoseasonality reconstructions based on shells of *P. vesicularis* or other gryphaeid shells that
829   contain multiple microstructures should benefit from the application of a multi-proxy approach that
830   allows the interpretation of seasonally changing environmental parameters. However, selective
831   diagenetic overprinting, the occurrence of growth cessations and the complexity of synchronizing
832   proxy records from multiple methods can complicate the interpretation of phase relationships
833   between proxies. Multi-proxy analysis on one exceptionally well-preserved specimen demonstrates
834   how the timing of seasonal deposition of the shell could be determined from the phase relationships
835   between proxies. Stable and clumped isotope records of primary foliated calcite in the hinge of *P.*
836   *vesicularis* yield a $\delta^{18}O_{seawater}$ of -2.8‰ indicative of seasonal freshwater input into the Neuquén
837   Basin. Mean annual sea water temperatures were 11°C based on clumped isotope thermometry,
838   which is much lower than reconstructions based on contextual TEX_{86}^H palaeothermometry (27.3°C ±
839   2.5°C). We conclude that the TEX_{86}^H method likely overestimates mean annual temperatures in this
840   setting, possibly representing summer surface water temperatures. Clumped isotope thermometry
841   of bulk foliated calcite samples likely underestimates the annual mean because the warm spring and
842   early summer season is underrepresented in the shells due to slower growth or growth cessations. A
843   seasonality in $\delta^{18}O$ of about 1‰ is ascribed to a combination of decreased salinity by fresh water
844   input in the summer season and a moderate temperature seasonality. Attempts to verify the
845   seasonality in SST by Mg/Ca ratios of shell calcite are complicated by uncertainties about vital effects
846   on the incorporation of Mg into the bivalve shell. Records of Zn/Ca, S/Ca and $\delta^{13}C$ show that the
847   warm, low salinity summer season is followed by a peak in productivity which influenced the
848   chemistry of the sea water in which *P. vesicularis* lived. The reconstruction of temperature
849   seasonality from fossil bivalve calcite is complicated by the influence of other palaeoenvironmental
850   parameters that affect the chemistry of bivalve shells. Yet, the successful application of clumped
851   isotope thermometry on fossil bivalve calcite in this study indicates that temperature seasonality in
852   fossil ostreid bivalves may be constrained by the sequential analysis of foliated calcite samples using
853   this method.

854

References

Abele, D., Brey, T., Philipp, E., Bivalve models of aging and the determination of molluscan lifespans. Experimental gerontology 44, 307–315, 2009.

Al-Aasm, I.S., Veizer, J., Diagenetic stabilization of aragonite and low-Mg calcite, I. Trace elements in rudists. Journal of Sedimentary Research 56, 1986a.

Al-Aasm, I.S., Veizer, J., Diagenetic stabilization of aragonite and low-Mg calcite, II. Stable isotopes in rudists. Journal of Sedimentary Research 56, 1986b.

Andrews, J.E., Tandon, S.K., Dennis, P.F., Concentration of carbon dioxide in the Late Cretaceous atmosphere. Journal of the Geological Society 152, 1–3, 1995.

Ayyasami, K., Role of oysters in biostratigraphy: A case study from the Cretaceous of the Ariyalur area, southern India. Geosciences Journal 10, 237–247, 2006.

Baldoni, A.M., Palynology of the lower lefipan formation (upper cretaceous) of barranca de los perros, chubut province, Argentina. part I. Cryptogam spores and gymnosperm pollen. Palynology 16, 117–136, 1992.

Banner, J.L., Hanson, G.N., Calculation of simultaneous isotopic and trace element variations during water-rock interaction with applications to carbonate diagenesis. Geochimica et Cosmochimica Acta 54, 3123–3137, 1990.

Barbin, V., Cathodoluminescence of carbonate shells: biochemical vs diagenetic process, in: Cathodoluminescence in Geosciences. Springer, pp. 303–329, 2000.

Barreda, V., Palazzesi, L., Patagonian vegetation turnovers during the Paleogene-early Neogene: origin of arid-adapted floras. The botanical review 73, 31–50, 2007.

Barreda, V.D., Cúneo, N.R., Wilf, P., Currano, E.D., Scasso, R.A., Brinkhuis, H., Cretaceous/Paleogene floral turnover in Patagonia: drop in diversity, low extinction, and a *Classopollis* spike. PLoS One 7, e52455, 2012.

Berner, R., Atmospheric carbon dioxide levels over Phanerozoic time. Science 249, 1382–1386, 1990.

Bertels, A.,. Micropaleontología y estratigrafía del límite Cretácico-Terciario en Huantrai-co (provincia de Neuquén). Ostracoda. Parte 1: Cytherellidae, Bairdiidae, Pontocypridinae, Buntoniinae y Trachyleberidinae (pro parte). Ameghiniana 5, 279–298, 2013.

Bieler, R., Mikkelsen, P.M., Lee, T., Foighil, D.Ó., Discovery of the Indo-Pacific oyster *Hyotissa hyotis* (Linnaeus, 1758) in the Florida Keys (Bivalvia: Gryphaeidae). Molluscan Research 24, 149–159, 2004.

Brand, U., Veizer, J., Chemical diagenesis of a multicomponent carbonate system–1: Trace elements. Journal of Sedimentary Research 50, 1980.

Brezina, S.S., Romero, M.V., Casadío, S., Bremec, C., Boring Polychaetes Associated with *Pycnodonte* (Phygraea) *vesicularis* (Lamarck) from the Upper Cretaceous of Patagonia. A Case of Commensalism? Ameghiniana 51, 129–140, 2014.

Brugger, J., Feulner, G., Petri, S., Baby, it's cold outside: Climate model simulations of the effects of the asteroid impact at the end of the Cretaceous: Chicxulub impact cooling. Geophysical Research Letters 44, 419–427. doi:10.1002/2016GL072241, 2017

Butler, P.G., Wanamaker, A.D., Scourse, J.D., Richardson, C.A., Reynolds, D.J., Variability of marine climate on the North Icelandic Shelf in a 1357-year proxy archive based on growth increments in the bivalve *Arctica islandica*. Palaeogeography, Palaeoclimatology, Palaeoecology 373, 141–151, 2013.

Calmano, W., Hong, J., Förstner, U., Binding and mobilization of heavy metals in contaminated sediments affected by pH and redox potential. Water science and technology 28, 223–235, 1993.

Calvert, S.E., Pedersen, T.F., Geochemistry of Recent oxic and anoxic marine sediments: Implications for the geological record. Marine Geology, Marine Sediments, Burial, Pore Water Chemistry, Microbiology and Diagenesis 113, 67–88. doi:10.1016/0025-3227(93)90150-T, 1993

Carré, M., Bentaleb, I., Blamart, D., Ogle, N., Cardenas, F., Zevallos, S., Kalin, R.M., Ortlieb, L., Fontugne, M., Stable isotopes and sclerochronology of the bivalve *Mesodesma donacium*: potential application to Peruvian paleoceanographic reconstructions. Palaeogeography, Palaeoclimatology, Palaeoecology 228, 4–25, 2005.

Carriker, Melbourne R., Palmer, R.E., Sick, L.V., Johnson, C.C., Interaction of mineral elements in sea water and shell of oysters (Crassostrea virginica (Gmelin)) cultured in controlled and natural systems. Journal of experimental marine biology and ecology 46, 279–296, 1980a.

Carriker, M.R., Palmer, R.E., Prezant, R.S., Ultrastructural morphogenesis of prodissoconch and early dissoconch valves of the oyster *Crassostrea virginica*. College of Marine Studies, University of Delaware, 1980b.

Chauvaud, L., Lorrain, A., Dunbar, R.B., Paulet, Y.-M., Thouzeau, G., Jean, F., Guarini, J.-M., Mucciarone, D., Shell of the Great Scallop *Pecten maximus* as a high-frequency archive of paleoenvironmental changes. Geochemistry, Geophysics, Geosystems 6, 2005.

Chinzei, K., Seilacher, A., Remote Biomineralization I: Fill skeletons in vesicular oyster shells.(With 7 figures in the text). Neues Jahrbuch fur Geologie und Palaontologie-Abhandlungen 190, 349–362, 1993.

Coggon, R.M., Teagle, D.A., Smith-Duque, C.E., Alt, J.C., Cooper, M.J., Reconstructing past seawater Mg/Ca and Sr/Ca from mid-ocean ridge flank calcium carbonate veins. Science 327, 1114–1117, 2010.

Crippa, G., Angiolini, L., Bottini, C., Erba, E., Felletti, F., Frigerio, C., Hennissen, J.A.I., Leng, M.J., Petrizzo, M.R., Raffi, I., Seasonality fluctuations recorded in fossil bivalves during the early Pleistocene: implications for climate change. Palaeogeography, Palaeoclimatology, Palaeoecology 446, 234–251, 2016.

Daëron, M., Blamart, D., Peral, M., Affek, H.P., Absolute isotopic abundance ratios and the accuracy of Δ_{47} measurements. Chemical Geology 442, 83–96, 2016.

Dale, A., John, C.M., Mozley, P.S., Smalley, P.C., Muggeridge, A.H., Time-capsule concretions: unlocking burial diagenetic processes in the Mancos Shale using carbonate clumped isotopes. Earth and Planetary Science Letters 394, 30–37, 2014.

de Winter, N.J., Zeeden, C., Hilgen, F.J., Low-latitude climate variability in the Heinrich frequency band of the Late Cretaceous greenhouse world. Climate of the Past 10, 1001–1015. doi:10.5194/cp-10-1001-2014, 2014.

de Winter, N.J., Claeys, P., Micro X-ray fluorescence (µXRF) line scanning on Cretaceous rudist bivalves: A new method for reproducible trace element profiles in bivalve calcite. Sedimentology. doi:10.1111/sed.12299, 2016.

de Winter, N.J., Goderis, S., Dehairs, F., Jagt, J.W.M., Fraaije, R.H.B., Van Malderen, S.J.M., Vanhaecke, F., Claeys, P., Tropical seasonality in the late Campanian (Late Cretaceous): Comparison between multiproxy records from three bivalve taxa from Oman. Palaeogeography, Palaeoclimatology, Palaeoecology, https://doi.org/10.1016/j.palaeo.2017.07.031, 2017a.

de Winter, N.J., Sinnesael, M., Makarona, C., Vansteenberge, S., Claeys, P., Trace element analyses of carbonates using portable and micro-X-ray fluorescence: Performance and optimization of measurement parameters and strategies. Journal of Analytical Atomic Spectrometry, 2017b.

Defliese, W.F., Hren, M.T., Lohmann, K.C., Compositional and temperature effects of phosphoric acid fractionation on Δ_{47} analysis and implications for discrepant calibrations. Chemical Geology 396, 51–60, 2015.

Dettman, D.L., Kohn, M.J., Quade, J., Ryerson, F.J., Ojha, T.P., Hamidullah, S., Seasonal stable isotope evidence for a strong Asian monsoon throughout the past 10.7 Myr. Geology 29, 31–34, 2001.

Dettman, D.L., Lohmann, K.C., Seasonal Change in Paleogene Surface Water δ^{18}O: Fresh-Water Bivalves of Western North America. Climate change in continental isotopic records 153–163, 1993.

Dettman, D.L., Lohmann, K.C., Oxygen isotope evidence for high-altitude snow in the Laramide Rocky Mountains of North America during the Late Cretaceous and Paleogene. Geology 28, 243–246. doi:10.1130/0091-7613(2000)28<243:OIEFHS>2.0.CO;2, 2000.

Dlugokencky, E., Tans P., NOAA/ESRL (www.esrl.noaa.gov/gmd/ccgg/trends/), accessed 31/01/2017.

Dodd, J.R., Crisp, E.L., Non-linear variation with salinity of Sr/Ca and Mg/Ca ratios in water and aragonitic bivalve shells and implications for paleosalinity studies. Palaeogeography, Palaeoclimatology, Palaeoecology 38, 45–56, 1982.

Donnadieu, Y., Pierrehumbert, R., Jacob, R., Fluteau, F., Modelling the primary control of paleogeography on Cretaceous climate. Earth and Planetary Science Letters 248, 426–437. doi:10.1016/j.epsl.2006.06.007, 2006

Dreier, A., Loh, W., Blumenberg, M., Thiel, V., Hause-Reitner, D., Hoppert, M., The isotopic biosignatures of photo-vs. thiotrophic bivalves: are they preserved in fossil shells? Geobiology 12, 406–423, 2014.

Duinker, J.C., Nolting, R.F., Michel, D., Effects of salinity, pH and redox conditions on the behaviour of Cd, Zn, Ni and Mn in the Scheldt estuary. Thalassia Jugosl 18, 191–202, 1982.

Dunbar, R.B., Wefer, G., Stable isotope fractionation in benthic foraminifera from the Peruvian continental margin. Marine Geology 59, 215–225, 1984.

Ekart, D.D., Cerling, T.E., Montanez, I.P., Tabor, N.J., A 400 million year carbon isotope record of pedogenic carbonate: implications for paleoatmospheric carbon dioxide. American Journal of Science 299, 805–827, 1999.

Elliot, M., Welsh, K., Chilcott, C., McCulloch, M., Chappell, J., Ayling, B., Profiles of trace elements and stable isotopes derived from giant long-lived *Tridacna gigas* bivalves: potential applications in paleoclimate studies. Palaeogeography, Palaeoclimatology, Palaeoecology 280, 132–142, 2009.

Folk, R.L., Land, L.S., Mg/Ca ratio and salinity: two controls over crystallization of dolomite. AAPG bulletin 59, 60–68, 1975.

Fossilworks.org: Pycnodonte genus, age range and distribution. Retrieved 14-02-2017

Freitas, P., Clarke, L.J., Kennedy, H., Richardson, C., Abrantes, F., Mg/Ca, Sr/Ca, and stable-isotope (δ^{18}O and δ^{13}C) ratio profiles from the fan mussel *Pinna nobilis* : Seasonal records and temperature relationships: *Pinna Nobilis* RATIO PROFILES. Geochemistry, Geophysics, Geosystems 6, n/a-n/a. doi:10.1029/2004GC000872, 2005

Freitas, P.S., Clarke, L.J., Kennedy, H., Richardson, C.A., Abrantes, F., Environmental and biological controls on elemental (Mg/Ca, Sr/Ca and Mn/Ca) ratios in shells of the king scallop *Pecten maximus*. Geochimica et Cosmochimica Acta 70, 5119–5133. doi:10.1016/j.gca.2006.07.029, 2006.

Freitas, P.S., Clarke, L.J., Kennedy, H.A., Richardson, C.A., Inter-and intra-specimen variability masks reliable temperature control on shell Mg/Ca ratios in laboratory and field cultured *Mytilus edulis* and *Pecten maximus* (bivalvia). Biogeosciences Discussions 5, 531–572, 2008.

Friedrich, O., Norris, R.D., Erbacher, J., Evolution of middle to Late Cretaceous oceans—a 55 my record of Earth's temperature and carbon cycle. Geology 40, 107–110, 2012.

Geist, J., Auerswald, K., Boom, A., Stable carbon isotopes in freshwater mussel shells: Environmental record or marker for metabolic activity? Geochimica et Cosmochimica Acta 69, 3545–3554, 2005.

Gillikin, D.P., De Ridder, F., Ulens, H., Elskens, M., Keppens, E., Baeyens, W., Dehairs, F., Assessing the reproducibility and reliability of estuarine bivalve shells (*Saxidomus giganteus*) for sea surface temperature reconstruction: implications for paleoclimate studies. Palaeogeography, Palaeoclimatology, Palaeoecology 228, 70–85, 2005a.

Gillikin, D.P., Lorrain, A., Navez, J., Taylor, J.W., André, L., Keppens, E., Baeyens, W., Dehairs, F., Strong biological controls on Sr/Ca ratios in aragonitic marine bivalve shells. Geochemistry, Geophysics, Geosystems 6, 2005b.

Gillikin, D.P., Lorrain, A., Bouillon, S., Willenz, P., Dehairs, F., Stable carbon isotopic composition of Mytilus edulis shells: relation to metabolism, salinity, δ^{13}C$_{DIC}$ and phytoplankton. Organic Geochemistry 37, 1371–1382, 2006.

Gillikin, D.P., Lorrain, A., Meng, L., Dehairs, F., A large metabolic carbon contribution to the δ^{13}C record in marine aragonitic bivalve shells. Geochimica et Cosmochimica Acta 71, 2936–2946, 2007.

Gillikin, D.P., Lorrain, A., Paulet, Y.-M., André, L., Dehairs, F., Synchronous barium peaks in high-resolution profiles of calcite and aragonite marine bivalve shells. Geo-Marine Letters 28, 351–358, 2008.

Goodwin, D.H., Flessa, K.W., Schöne, B.R., Dettman, D.L., Cross-calibration of daily growth increments, stable isotope variation, and temperature in the Gulf of California bivalve mollusk *Chione cortezi*: implications for paleoenvironmental analysis. Palaios 16, 387–398, 2001.

Grossman, E.L., Ku, T.-L., Oxygen and carbon isotope fractionation in biogenic aragonite: temperature effects. Chemical Geology: Isotope Geoscience section 59, 59–74, 1986.

Guo, T., DeLaune, R.D., Patrick, W.H., The influence of sediment redox chemistry on chemically active forms of arsenic, cadmium, chromium, and zinc in estuarine sediment. Environment International 23, 305–316, 1997.

Gutiérrez-Zugasti, I., Clarke, L.J., Garcia-Escárzaga, A., Suárez-Revilla, R., G.N., González-Morales, M. Changes in seawater temperatures in northern Iberia during the Late Pleistocene and Early Holocene. 22nd Annual Meeting of the EAA 2016, TH5-13, Abstract 4, September 3, 2016.

Habermann, D., Quantitative cathodoluminescence (CL) spectroscopy of minerals: possibilities and limitations. Mineralogy and Petrology 76, 247–259, 2002.

Hallmann, N., Burchell, M., Brewster, N., Martindale, A., Schöne, B.R., Holocene climate and seasonality of shell collection at the Dundas Islands Group, northern British Columbia, Canada—A bivalve sclerochronological approach. Palaeogeography,

Palaeoclimatology, Palaeoecology 373, 163–172, 2013.

Harzhauser, M., Piller, W.E., Müllegger, S., Grunert, P., Micheels, A., Changing seasonality patterns in Central Europe from Miocene Climate Optimum to Miocene Climate Transition deduced from the *Crassostrea* isotope archive. Global and Planetary Change 76, 77–84, 2011.

Hay, W.W., Evolving ideas about the Cretaceous climate and ocean circulation. Cretaceous Research 29, 725–753, 2008.

Hay, 2013

Hayami, I., Kase, T., A new cryptic species of *Pycnodonte* from Ryukyu Islands: a living fossil oyster. Nihon Koseibutsu Gakkai hokoku, kiji 1070–1089, 1992.

Hays, P.D., Grossman, E.L., Oxygen isotopes in meteoric calcite cements as indicators of continental paleoclimate. Geology 19, 441–444. https://doi.org/10.1130/0091-7613(1991)019<0441:OIIMCC>2.3.CO;2, 1991.

Huber, B.T., Norris, R.D., MacLeod, K.G., Deep-sea paleotemperature record of extreme warmth during the Cretaceous. Geology 30, 123–126. doi:10.1130/0091-7613(2002)030<0123:DSPROE>2.0.CO;2, 2002.

Hunter, S.J., Valdes, P.J., Haywood, A.M., Markwick, P.J., Modelling Maastrichtian climate: investigating the role of geography, atmospheric CO_2 and vegetation. Climate of the Past Discussions 4, 981–1019, 2008.

Huntington, K.W., Budd, D.A., Wernicke, B.P., Eiler, J.M., Use of clumped-isotope thermometry to constrain the crystallization temperature of diagenetic calcite. Journal of Sedimentary Research 81, 656–669, 2011.

Iglesias, A., Wilf, P., Johnson, K.R., Zamuner, A.B., Cúneo, N.R., Matheos, S.D., Singer, B.S., A Paleocene lowland macroflora from Patagonia reveals significantly greater richness than North American analogs. Geology 35, 947–950, 2007.

IPCC: Climate Change 2014: Synthesis Report. Contribution of Working Groups I, II and III to the Fifth Assessment Report of the Intergovernmental Panel on Climate Change [Core Writing Team, R.K. Pachauri and L.A. Meyer (eds.)]. IPCC, Geneva, Switzerland, 151 pp, 2014.

Jackson, L.J., Kalff, J., Rasnnussen, J.B., Sediment pH and redox potential affect the bioavailability of Al, Cu, Fe, Mn, and Zn to rooted aquatic macrophytes. Canadian Journal of Fisheries and Aquatic Sciences 50, 143–148, 1993.

Jia, G., X. Wang, W. Guo, and L. Dong, Seasonal distribution of archaeal lipids in surface water and its constraint on their sources and the TEX_{86} temperature proxy in sediments of the South China Sea, J. Geophys. Res. Biogeosci., 122, doi:10.1002/2016JG003732, 2017.

Jones, D.S., Annual cycle of shell growth increment formation in two continental shelf bivalves and its paleoecologic significance. Paleobiology 6, 331–340, 1980.

Jones, D.S., Sclerochronology: reading the record of the molluscan shell: annual growth increments in the shells of bivalve molluscs record marine climatic changes and reveal surprising longevity. American Scientist 71, 384–391, 1983.

Kiessling, W., Aragón, E., Scasso, R., Aberhan, M., Kriwet, J., Medina, F., Fracchia, D., Massive corals in Paleocene siliciclastic sediments of Chubut (Argentina). Facies 51, 233–241, 2005.

Kirby, M.X., Soniat, T.M., Spero, H.J., Stable isotope sclerochronology of Pleistocene and Recent oyster shells (*Crassostrea virginica*). Palaios 13, 560–569, 1998.

Kirby, M.X., Paleoecological differences between Tertiary and Quaternary *Crassostrea* oysters, as revealed by stable isotope sclerochronology. Palaios 15, 132–141, 2000.

Klein, R.T., Lohmann, K.C., Thayer, C.W., Bivalve skeletons record sea-surface temperature and $\delta^{18}O$ via Mg/Ca and $^{18}O/^{16}O$ ratios. Geology 24, 415–418, 1996a.

Klein, R.T., Lohmann, K.C., Thayer, C.W., Sr/Ca and $^{13}C^{12}C$ ratios in skeletal calcite of *Mytilus trossulus*: Covariation with metabolic rate, salinity, and carbon isotopic composition of seawater. Geochimica et Cosmochimica Acta 60, 4207–4221, 1996b.

Klein, J.S., Mozley, P., Campbell, A., Cole, R., Spatial distribution of carbon and oxygen isotopes in laterally extensive carbonate-cemented layers: implications for mode of growth and subsurface identification. Journal of Sedimentary Research 69, 1999.

Langlet, D., Alunno-Bruscia, M., Rafélis, M., Renard, M., Roux, M., Schein, E., Buestel, D., Experimental and natural cathodoluminescence in the shell of *Crassostrea gigas* from Thau lagoon (France): ecological and environmental implications. Marine Ecology Progress Series 317, 143–156, 2006.

Lartaud, F., De Rafélis, M., Ropert, M., Emmanuel, L., Geairon, P., Renard, M., Mn labelling of living oysters: artificial and natural cathodoluminescence analyses as a tool for age and growth rate determination of *C. gigas* (Thunberg, 1793) shells. Aquaculture 300, 206–217, 2010a.

Lartaud, F., Emmanuel, L., De Rafélis, M., Pouvreau, S., Renard, M., Influence of food supply on the $\delta^{13}C$ signature of mollusc shells: implications for palaeoenvironmental reconstitutions. Geo-Marine Letters 30, 23–34, 2010b.

Lazareth, C.E., Vander Putten, E., André, L., Dehairs, F., High-resolution trace element profiles in shells of the mangrove bivalve *Isognomon ephippium*: a record of environmental spatio-temporal variations? Estuarine, Coastal and Shelf Science 57, 1103–1114, 2003.

Lear, C.H., Elderfield, H., Wilson, P.A., Cenozoic deep-sea temperatures and global ice volumes from Mg/Ca in benthic foraminiferal calcite. Science 287, 269–272, 2000.

Lear, C.H., Coxall, H.K., Foster, G.L., Lunt, D.J., Mawbey, E.M., Rosenthal, Y., Sosdian, S.M., Thomas, E., Wilson, P.A., Neogene ice volume and ocean temperatures: Insights from infaunal foraminiferal Mg/Ca paleothermometry. Paleoceanography 30, 1437–1454, 2015.

Lécuyer, C., Reynard, B., Martineau, F., Stable isotope fractionation between mollusc shells and marine waters from Martinique Island. Chemical Geology 213, 293–305, 2004.

Linnaeus, Carolus, Systema naturae per regna tria naturae : secundum classes, ordines, genera, species, cum characteribus, differentiis, synonymis, locis., 10th edition, Lars Salvi, Stockholm, 1758

Lorens, R.B., Bender, M.L., The impact of solution chemistry on *Mytilus edulis* calcite and aragonite. Geochimica et Cosmochimica Acta 44, 1265–1278, 1980.

Lorrain, A., Paulet, Y.-M., Chauvaud, L., Dunbar, R., Mucciarone, D., Fontugne, M., $\delta^{13}C$ variation in scallop shells: increasing metabolic carbon contribution with body size? Geochimica et Cosmochimica Acta 68, 3509–3519, 2004.

Lorrain, A., Gillikin, D.P., Paulet, Y.-M., Chauvaud, L., Le Mercier, A., Navez, J., André, L., Strong kinetic effects on Sr/Ca ratios in the calcitic bivalve *Pecten maximus*. Geology 33, 965–968, 2005.

Loyd, S.J., Corsetti, F.A., Eiler, J.M., Tripati, A.K., Determining the diagenetic conditions of concretion formation: assessing temperatures and pore waters using clumped isotopes. Journal of Sedimentary Research 82, 1006–1016, 2012.

MacDonald, J., Freer, A., Cusack, M., Alignment of crystallographic c-axis throughout the four distinct microstructural layers of the oyster *Crassostrea gigas*. Crystal Growth & Design 10, 1243–1246, 2009.

Machel, H.G., Burton, E.A., Factors governing cathodoluminescence in calcite and dolomite, and their implications for studies of carbonate diagenesis, 1991.

Malumian, N., Nanez, C., The Late Cretaceous–Cenozoic transgressions in Patagonia and the Fuegian Andes: foraminifera, palaeoecology,

1076   and palaeogeography. Biological Journal of the Linnean Society 103, 269–288, 2011.
1077   Marali, S., Schöne, B.R., Oceanographic control on shell growth of *Arctica islandica* (Bivalvia) in surface waters of Northeast Iceland—
1078   Implications for paleoclimate reconstructions. Palaeogeography, Palaeoclimatology, Palaeoecology 420, 138–149, 2015.
1079   Marali, S., Schöne, B.R., Mertz-Kraus, R., Griffin, S.M., Wanamaker, A.D., Matras, U., Butler, P.G., Ba/Ca ratios in shells of *Arctica*
1080   *islandica*—Potential environmental proxy and crossdating tool. Palaeogeography, Palaeoclimatology, Palaeoecology 465, 347–
1081   361, 2017.
1082   McConnaughey, T., ^{13}C and ^{18}O isotopic disequilibrium in biological carbonates: II. In vitro simulation of kinetic isotope effects, 1989.
1083   Geochimica et Cosmochimica Acta 53, 163–171.
1084   McConnaughey, T.A., Burdett, J., Whelan, J.F., Paull, C.K., Carbon isotopes in biological carbonates: Respiration and photosynthesis.
1085   Geochimica et Cosmochimica Acta 61, 611–622. doi:10.1016/S0016-7037(96)00361-4, 1997.
1086   McConnaughey, T.A., Gillikin, D.P., Carbon isotopes in mollusk shell carbonates. Geo-Marine Letters 28, 287–299, 2008.
1087   Miller, K.G., Sugarman, P.J., Browning, J.V., Kominz, M.A., Hernández, J.C., Olsson, R.K., Wright, J.D., Feigenson, M.D., Van Sickel,
1088   W., Late Cretaceous chronology of large, rapid sea-level changes: Glacioeustasy during the greenhouse world. Geology 31, 585–
1089   588, 2003.
1090   Morrison, J.M., Codispoti, L.A., Gaurin, S., Jones, B., Manghnani, V., Zheng, Z., Seasonal variation of hydrographic and nutrient fields
1091   during the US JGOFS Arabian Sea Process Study. Deep Sea Research Part II: Topical Studies in Oceanography 45, 2053–2101,
1092   1998.
1093   Mouchi, V., De Rafélis, M., Lartaud, F., Fialin, M., Verrecchia, E., Chemical labelling of oyster shells used for time-calibrated high-
1094   resolution Mg/Ca ratios: a tool for estimation of past seasonal temperature variations. Palaeogeography, Palaeoclimatology,
1095   Palaeoecology 373, 66–74, 2013.
1096   Müller, A.H., Zur funktionellen Morphologie, Taxiologie und Ökologie von Pycnodonta (Ostreina, Lamellibranchiata). Monatsberichte der
1097   Deutschen Akademie der Wissenschaften zu Berlin 12, 902–923, 1970.
1098   Nestler, H., Entwicklung und Schalenstruktur von *Pycnodonte uesicularis* (LAM.) und *Dimyodon nilssoni* (v. Hag.) aus der Oberkreide.
1099   Geologie L4 64–77, 1965.
1100   O'Brien, C.L., Robinson, S.A., Pancost, R.D., Sinninghe Damsté, J.S., Schouten, S., Lunt, D.J., Alsenz, H., Bornemann, A., Bottini, C.,
1101   Brassell, S.C., Farnsworth, A., Forster, A., Huber, B.T., Inglis, G.N., Jenkyns, H.C., Linnert, C., Littler, K., Markwick, P.,
1102   McAnena, A., Mutterlose, J., Naafs, B.D.A., Püttmann, W., Sluijs, A., van Helmond, N.A.G.M., Vellekoop, J., Wagner, T.,
1103   Wrobel, N.E., Cretaceous sea-surface temperature evolution: Constraints from TEX$_{86}$ and planktonic foraminiferal oxygen
1104   isotopes. Earth-Science Reviews 172, 224–247. doi:10.1016/j.earscirev.2017.07.012, 2017.
1105   Omata, T., Suzuki, A., Kawahat, H., Okamoto, M., Annual fluctuation in the stable carbon isotope ratio of coral skeletons: the relative
1106   intensities of kinetic and metabolic isotope effects. Geochimica et cosmochimica acta 69, 3007–3016, 2005.
1107   Otto-Bliesner, B.L., Brady, E.C., Shields, C., Late Cretaceous ocean: Coupled simulations with the National Center for Atmospheric
1108   Research Climate System Model. J. Geophys. Res. 107, ACL 11-1. doi:10.1029/2001JD000821, 2002.
1109   Owen, R., Kennedy, H., Richardson, C., Experimental investigation into partitioning of stable isotopes between scallop (*Pecten maximus*)
1110   shell calcite and sea water. Palaeogeography, Palaeoclimatology, Palaeoecology 185, 163–174, 2002.
1111   Palazzesi, L., Barreda, V., Major vegetation trends in the Tertiary of Patagonia (Argentina): a qualitative paleoclimatic approach based on
1112   palynological evidence. Flora-Morphology, Distribution, Functional Ecology of Plants 202, 328–337, 2007.
1113   Pearson, P.N., Ditchfield, P.W., Singano, J., Harcourt-Brown, K.G., Nicholas, C.J., Olsson, R.K., Shackleton, N.J., Hall, M.A., Warm
1114   tropical sea surface temperatures in the Late Cretaceous and Eocene epochs. Nature 413, 481–487, 2001.
1115   Pennington, J.T., Chavez, F.P., Seasonal fluctuations of temperature, salinity, nitrate, chlorophyll and primary production at station H3/M1
1116   over 1989–1996 in Monterey Bay, California. Deep Sea Research Part II: Topical Studies in Oceanography 47, 947–973, 2000.
1117   Petersen, S.V., Winkelstern, I.Z., Lohmann, K.C., Meyer, K.W., The effects of Porapak^{TM} trap temperature on δ^{18}O, δ^{13}C, and Δ_{47} values in
1118   preparing samples for clumped isotope analysis. Rapid Communications in Mass Spectrometry 30, 199–208, 2016.
1119   Pirrie, D., Marshall, J.D., Diagenesis of Inoceramus and Late Cretaceous paleoenvironmental geochemistry: a case study from James Ross
1120   Island, Antarctica. Palaios 336–345, 1990.
1121   Prámparo, M.B., Papu, O.H., Milana, J.P., Estudios palinológicos del miembro inferior de la Formación Pachaco, Terciano de la provincia
1122   de San Juan. Descripciones sistemáticas. Ameghiniana 33, 397–407, 1996.
1123   Prámparo, M.B., Papu, O.H., Late Maastrichtian dinoflagellate cysts from the Cerro Butaló section, southern Mendoza province, Argentina.
1124   Journal of Micropalaeontology 25, 23–33, 2006.
1125   Pugaczewska, H., The Upper Cretaceous Ostreidae from the Middle Vistula Region (Poland). Acta palaeontologica polonica 22, 1977.
1126   Quan, C., Sun, C., Sun, Y., Sun, G., High resolution estimates of paleo-CO$_2$ levels through the Campanian (Late Cretaceous) based on
1127   Ginkgo cuticles. Cretaceous Research 30, 424–428, 2009.
1128   Ravelo, A.C., Hillaire-Marcel, C., Chapter Eighteen the use of oxygen and carbon isotopes of foraminifera in Paleoceanography.
1129   Developments in Marine Geology 1, 735–764, 2007.
1130   Richardson, C.A., Peharda, M., Kennedy, H., Kennedy, P., Onofri, V., Age, growth rate and season of recruitment of *Pinna nobilis* (L) in
1131   the Croatian Adriatic determined from Mg: Ca and Sr: Ca shell profiles. Journal of Experimental Marine Biology and Ecology
1132   299, 1–16, 2004.
1133   Romanek, C.S., Grossman, E.L., Morse, J.W., Carbon isotopic fractionation in synthetic aragonite and calcite: effects of temperature and
1134   precipitation rate. Geochimica et Cosmochimica Acta 56, 419–430, 1992.
1135   Rosenberg, G.D., Hughes, W.W., A metabolic model for the determination of shell composition in the bivalve mollusc, *Mytilus edulis*.
1136   Lethaia 24, 83–96, 1991.
1137   Scasso, R.A., Concheyro, A., Kiessling, W., Aberhan, M., Hecht, L., Medina, F.A., Tagle, R., A tsunami deposit at the
1138   Cretaceous/Paleogene boundary in the Neuquén Basin of Argentina. Cretaceous Research 26, 283–297, 2005.
1139   Schauer, A.J., Kelson, J., Saenger, C., Huntington, K.W., Choice of 17O correction affects clumped isotope (Δ_{47}) values of CO$_2$ measured
1140   with mass spectrometry. Rapid Communications in Mass Spectrometry 30, 2607–2616, 2016.
1141   Schlager, W., James, N.P., Low-magnesian calcite limestones forming at the deep-sea floor, Tongue of the Ocean, Bahamas. Sedimentology
1142   25, 675–702, 1978.
1143   Schöne, B.R., Fiebig, J., Pfeiffer, M., Gleβ, R., Hickson, J., Johnson, A.L., Dreyer, W., Oschmann, W., Climate records from a bivalved
1144   Methuselah (*Arctica islandica*, Mollusca; Iceland). Palaeogeography, Palaeoclimatology, Palaeoecology 228, 130–148, 2005a.
1145   Schöne, B.R., Houk, S.D., Castro, A.D.F., Fiebig, J., Oschmann, W., Kröncke, I., Dreyer, W., Gosselck, F. Daily growth rates in shells of
1146   *Arctica islandica*: assessing sub-seasonal environmental controls on a long-lived bivalve mollusk. Palaios 20, 78–92, 2005b.
1147   Schöne, B.R., Pfeiffer, M., Pohlmann, T., Siegismund, F., A seasonally resolved bottom-water temperature record for the period AD 1866–
1148   2002 based on shells of *Arctica islandica* (Mollusca, North Sea). International Journal of Climatology 25, 947–962, 2005c.
1149   Servicio Meteorológico Nacional, Republic of Argentina,
1150   http://www.smn.gov.ar/serviciosclimaticos/?mod=turismo&id=5&var=buenosaires, visited on 25-09-2017.

1151 Schouten, S., Hopmans, E. C., & Damsté, J. S. S. The organic geochemistry of glycerol dialkyl glycerol tetraether lipids: a review. Organic
1152   geochemistry, 54, 19-61, 2013.
1153 Stanley, S.M., Hardie, L.A., Secular oscillations in the carbonate mineralogy of reef-building and sediment-producing organisms driven by
1154   tectonically forced shifts in seawater chemistry. Palaeogeography, Palaeoclimatology, Palaeoecology 144, 3–19, 1998.
1155 Stenzel, H. B. Cretaceous oysters of southwestern North America. Int. Geol. Congr. Mexico City, 15-37, 1956.
1156 Stenzel, H.B., Oysters. University of Kansas Press and Geological Society of America, Part N, Mollusca, 1971.
1157 Steuber, T., Stable isotope sclerochronology of rudist bivalves: Growth rates and Late Cretaceous seasonality. Geology 24, 315.
1158   doi:10.1130/0091-7613(1996)024<0315:SISORB>2.3.CO;2, 1996.
1159 Steuber, T., Isotopic and chemical intra-shell variations in low-Mg calcite of rudist bivalves (Mollusca-Hippuritacea): disequilibrium
1160   fractionations and late Cretaceous seasonality. International Journal of Earth Sciences 88, 551–570, 1999.
1161 Steuber, T., Rauch, M., Masse, J.-P., Graaf, J., Malkoč, M., Low-latitude seasonality of Cretaceous temperatures in warm and cold episodes.
1162   Nature 437, 1341–1344, 2005.
1163 Surge, D., Lohmann, K.C., Dettman, D.L., Controls on isotopic chemistry of the American oyster, *Crassostrea virginica*: implications for
1164   growth patterns. Palaeogeography, Palaeoclimatology, Palaeoecology 172, 283–296, 2001.
1165 Surge, D., Lohmann, K.C., Evaluating Mg/Ca ratios as a temperature proxy in the estuarine oyster, *Crassostrea virginica.* J. Geophys. Res.
1166   113, 2001. doi:10.1029/2007JG000623, 2008.
1167 Takesue, R.K., van Geen, A., Mg/Ca, Sr/Ca, and stable isotopes in modern and Holocene *Protothaca staminea* shells from a northern
1168   California coastal upwelling region. Geochimica et Cosmochimica Acta 68, 3845–3861, 2004.
1169 Titschack, J., Zuschin, M., Spötl, C., Baal, C., The giant oyster *Hyotissa hyotis* from the northern Red Sea as a decadal-scale archive for
1170   seasonal environmental fluctuations in coral reef habitats. Coral Reefs 29, 1061–1075, 2010.
1171 Torsvik, T.H., Van der Voo, R., Preeden, U., Mac Niocaill, C., Steinberger, B., Doubrovine, P.V., van Hinsbergen, D.J., Domeier, M.,
1172   Gaina, C., Tohver, E., Phanerozoic polar wander, palaeogeography and dynamics. Earth-Science Reviews 114, 325–368, 2012.
1173 Tripati, A., Zachos, J., Marincovich Jr., L., Bice, K., Late Paleocene Arctic coastal climate inferred from molluscan stable and radiogenic
1174   isotope ratios. Palaeogeography, Palaeoclimatology, Palaeoecology 170, 101–113. doi:10.1016/S0031-0182(01)00230-9, 2001.
1175 Ullmann, C.V., Wiechert, U., Korte, C., Oxygen isotope fluctuations in a modern North Sea oyster (*Crassostrea gigas*) compared with
1176   annual variations in seawater temperature: Implications for palaeoclimate studies. Chemical Geology 277, 160–166.
1177   doi:10.1016/j.chemgeo.2010.07.019, 2010.
1178 Ullmann, C.V., Böhm, F., Rickaby, R.E., Wiechert, U., Korte, C., The Giant Pacific Oyster (*Crassostrea gigas*) as a modern analog for
1179   fossil ostreoids: isotopic (Ca, O, C) and elemental (Mg/Ca, Sr/Ca, Mn/Ca) proxies. Geochemistry, Geophysics, Geosystems 14,
1180   4109–4120, 2013.
1181 van Hinsbergen, D.J., de Groot, L.V., van Schaik, S.J., Spakman, W., Bijl, P.K., Sluijs, A., Langereis, C.G., Brinkhuis, H., A paleolatitude
1182   calculator for paleoclimate studies. PloS one 10, e0126946, 2015.
1183 Van Rampelbergh, M., Verheyden, S., Allan, M., Quinif, Y., Keppens, E., Claeys, P., Seasonal variations recorded in cave monitoring
1184   results and a 10 year monthly resolved speleothem δ18O and δ13C record from the Han-sur-Lesse cave, Belgium. Climate of the
1185   Past Discussions 10, 1821–1856, 2014.
1186 Vander Putten, E., Dehairs, F., Keppens, E., Baeyens, W., High resolution distribution of trace elements in the calcite shell layer of modern
1187   *Mytilus edulis*: Environmental and biological controls. Geochimica et Cosmochimica Acta 64, 997–1011, 2000.
1188 Veizer, J., Chemical diagenesis of carbonates: theory and application of trace element technique, 1983.
1189 Vellekoop, J., Esmeray-Senlet, S., Miller, K.G., Browning, J.V., Sluijs, A., van de Schootbrugge, B., Damsté, J.S.S., Brinkhuis, H.,
1190   Evidence for Cretaceous-Paleogene boundary bolide "impact winter" conditions from New Jersey, USA. Geology 44, 619–622,
1191   2016.
1192 Vermeij, G.J., The oyster enigma variations: a hypothesis of microbial calcification. Paleobiology 40, 1–13, 2014.
1193 Videt, B. Dynamique des paléoenvironnements à huîtres du Crétacé supérieur nord-aquitain (SW France) et du Mio-Pliocène andalou (SE
1194   Espagne): biodiversité, analyse séquentielle, biogéochimie. – Mém. Géosc. Rennes, 108, 1-261, 2004.
1195 Wanamaker Jr, A.D., Kreutz, K.J., Wilson, T., Borns Jr, H.W., Introne, D.S., Feindel, S., Experimentally determined Mg/Ca and Sr/Ca
1196   ratios in juvenile bivalve calcite for *Mytilus edulis*: implications for paleotemperature reconstructions. Geo-Marine Letters 28,
1197   359–368, 2008.
1198 Wang, W.-X., Fisher, N.S., Assimilation of trace elements and carbon by the mussel *Mytilus edulis*: effects of food composition. Limnology
1199   and Oceanography 4, l, 1996.
1200 Wang, Q.J., Xu, X.H., Jin, P.H., Li, R.Y., Li, X.Q., Sun, B.N., Quantitative reconstruction of Mesozoic paleoatmospheric CO2 based on
1201   stomatal parameters of fossil *Baiera furcata* of Ginkgophytes. Geological review 59, 1035–1045, 2013.
1202 Watanabe, T., Winter, A., Oba, T., Seasonal changes in sea surface temperature and salinity during the Little Ice Age in the Caribbean Sea
1203   deduced from Mg/Ca and 18O/16O ratios in corals. Marine Geology 173, 21–35, 2001.
1204 Weiner, S., Dove, P.M., An overview of biomineralization processes and the problem of the vital effect. Reviews in mineralogy and
1205   geochemistry 54, 1–29, 2003.
1206 Wisshak, M., Correa, M.L., Gofas, S., Salas, C., Taviani, M., Jakobsen, J., Freiwald, A., Shell architecture, element composition, and stable
1207   isotope signature of the giant deep-sea oyster *Neopycnodonte zibrowii* sp. n. from the NE Atlantic. Deep Sea Research Part I:
1208   Oceanographic Research Papers 56, 374–407, 2009.
1209 Woelders, L., Vellekoop, J., Kroon, D., Smit, J., Casadío, S., Prámparo, M.B., Dinarès-Turell, J., Peterse, F., Sluijs, A., Lenaerts, J.T.M.,
1210   Speijer, R.P., Latest Cretaceous climatic and environmental change in the South Atlantic region. Paleoceanography
1211   2016PA003007. doi:10.1002/2016PA003007, 2017.
1212 Woo, K.-S., Anderson, T.F., Sandberg, P.A., Diagenesis of skeletal and nonskeletal components of mid-Cretaceous limestones. Journal of
1213   Sedimentary Research 63, 1993.
1214

1215

1216 [FIGURE CAPTIONS]
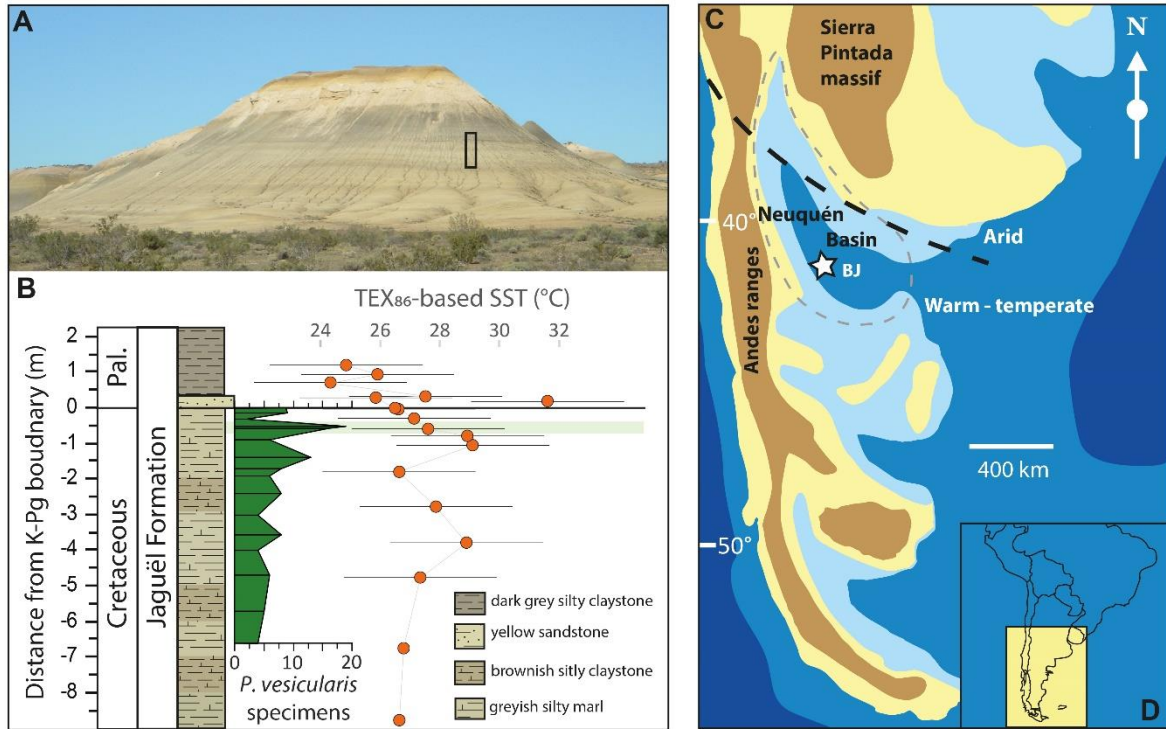
1217

1218 **Figure 1**

1219 Background information of the studied *Pycnodonte vesicularis* specimens. A) The Bajada de Jaguël
1220   section in outcrop (BJ; modern location: 38°06'10.5"S, 68°23'20.5"W, palaeolatitude = 43°S).
1221   B) lithology, stratigraphy and TEX$_{86}$ record (Woelders et al., 2017) of the BJ section. The main
1222   *P. vesicularis* level is indicated in light green. The abundance of *P. vesicularis* is based on
1223   Aberhan and Kiessling (2014). C) Palaeogeography of study area during the latest
1224   Cretaceous. Palaeomap after Scasso et al. (2005) and Woelders et al. (2017). D) Location of
1225   the study area in southern Argentina relative to modern day South America.
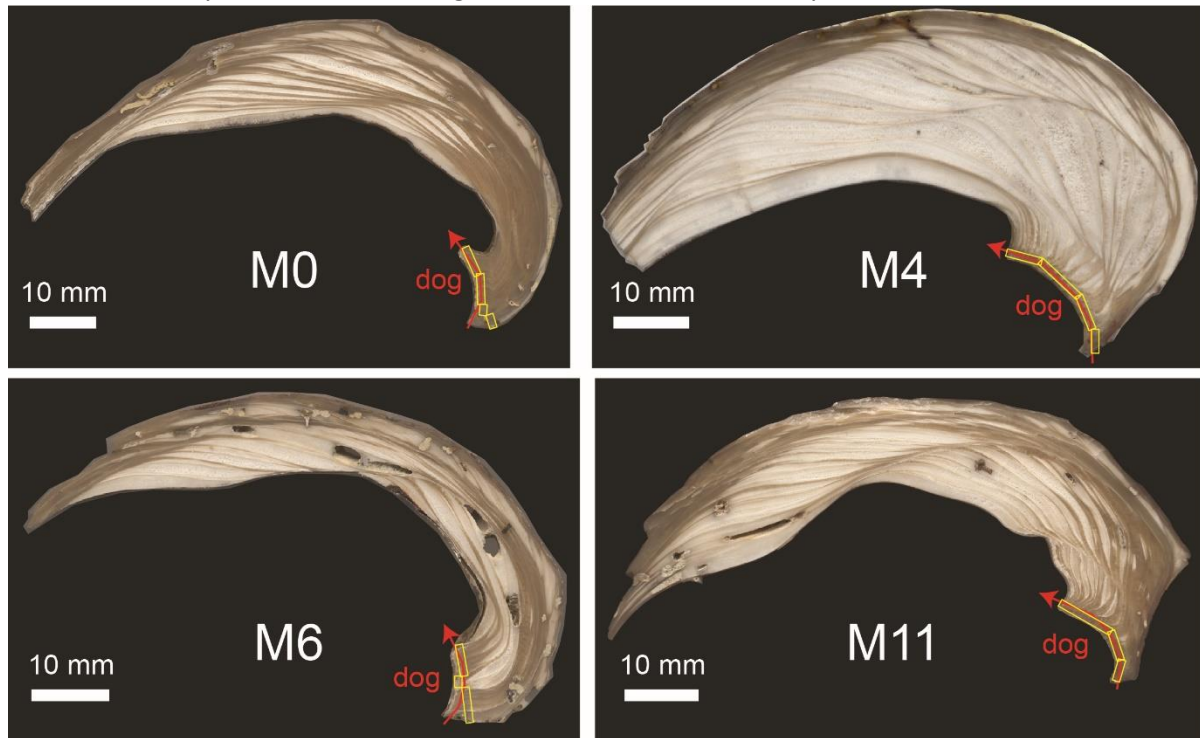
1226

1227 **Figure 2**

1228 Colour scans of cross sections of the four shells subject to multi-proxy analysis. Red arrows indicate
1229   sampling location and direction. Yellow boxes indicate the location of stable isotope
1230   transects. XRF sampling is in the direction of growth ("dog").
1231
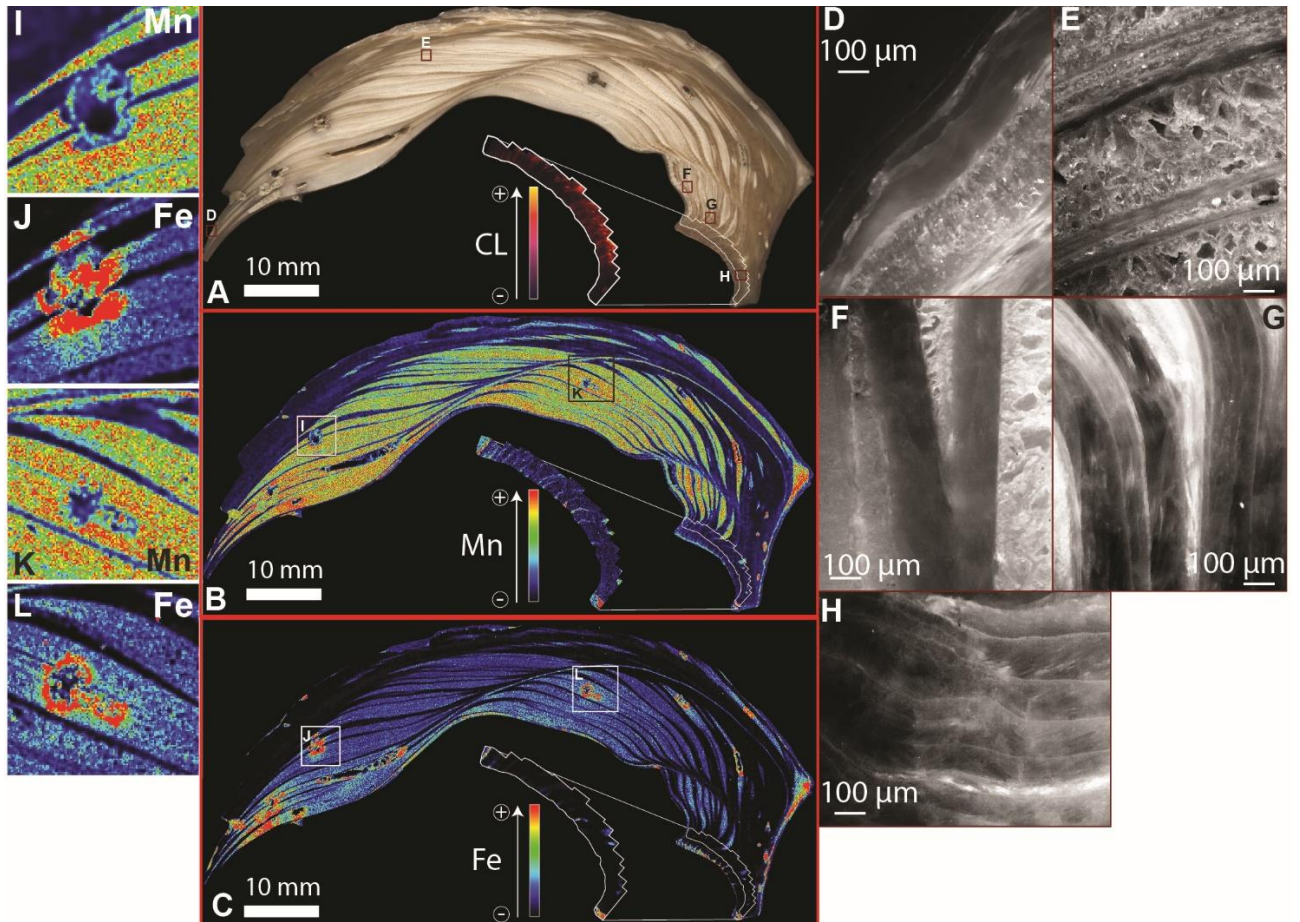
1232
1233 **Figure 3**
1234 Overview of the results of colour scanning, microscopic analyses and µXRF mapping of specimen
1235   M11. A) Colour scan of cross section in growth direction through the shell, with close-up of
1236   cathodoluminescence microscopic image of the hinge line. B) µXRF mapping of Mn the cross
1237   section, with close-up of the µXRF map of the hinge line. C) µXRF mapping of Fe the cross
1238   section, with close-up of the µXRF map of the hinge line. D) Micrograph of transitions
1239   between foliated and vesicular calcite near the edge of the shell. Note the blocky calcite
1240   crystals in the vesicular microstructure. E) Micrograph of thin, alternating layers of foliated
1241   and vesicular calcite. F) Micrograph showing sharp transitions between dense foliated calcite
1242   and porous vesicular calcite G) Micrograph of gradual transitions between foliated calcite
1243   and vesicular calcite closer to the hinge. H) Micrograph of dense, foliated calcite layers in
1244   shell hinge line. Note the thin layer of vesicular calcite (white) intercalated between the
1245   foliated layers near the bottom of the image. I-L) Close-ups of µXRF mapping of bore holes
1246   with coronas of elevated Fe and Mn concentrations.
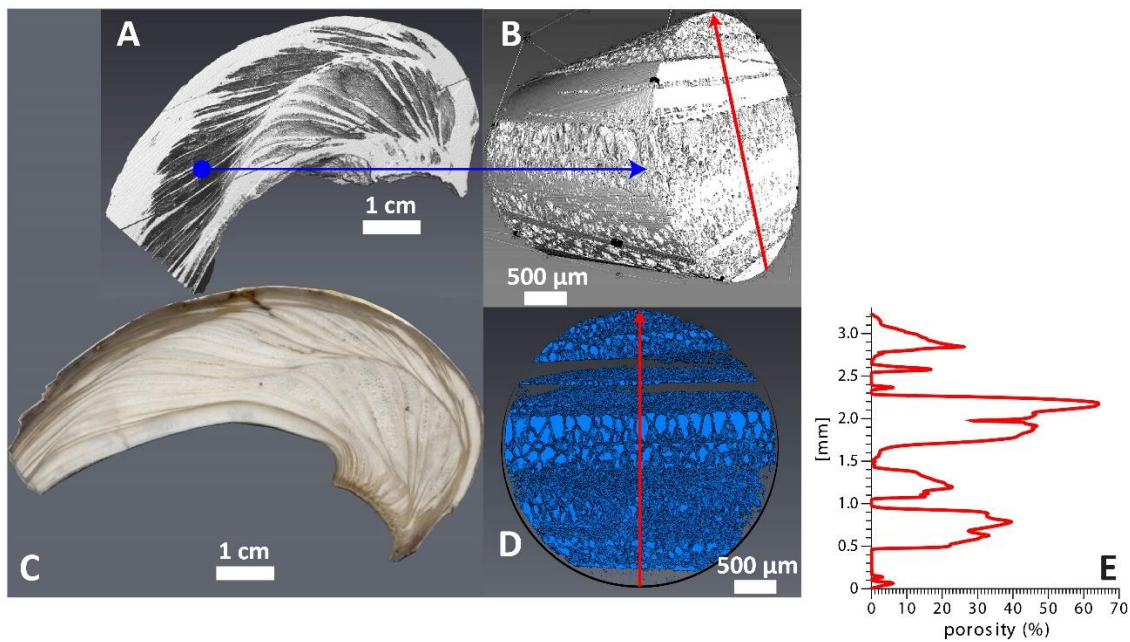
Figure 4

Overview of the results of CT-scanning and porosity analysis on specimen M4, with A) showing an
overview of density variations in the shell (white = dense calcite, darker colours represent
porosity). The blue dot shows the location of the part of the shell that was CT-scanned at
high resolution. B) shows the shape and density of a part of the shell that was CT-scanned
with higher spatial resolution as well as the location of the porograph shown in E). C) shows
a colour scan of the shell cross section. D) shows a high-resolution cross-section through the
shell with porosity in blue (light blue = porosity, darker colours = dense calcite). The red line
is in the same location as in B). E) shows a graph of porosity through the high resolution
section perpendicular to the growth layers.
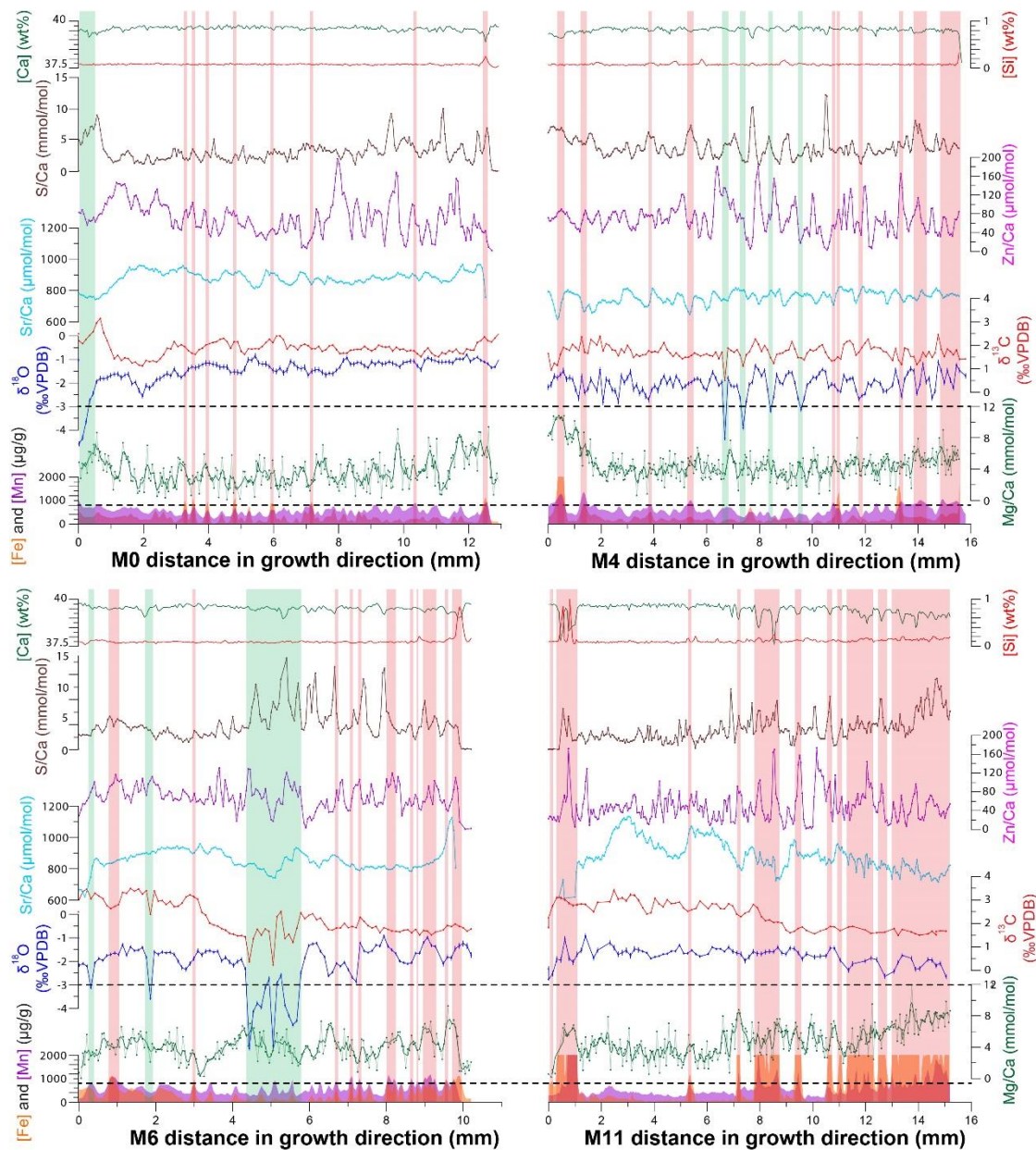
Figure 5

Overview of multi-proxy records through the hinges of 4 specimens of *P. vesicularis*. From top to bottom, records of [Ca] (green), [Si] (red), S/Ca ratios (brown), Zn/Ca ratios (purple), Sr/Ca ratios (light blue), δ^{13}C (red), δ^{18}O (blue), Mg/Ca (green), [Mn] (purple) and [Fe] (orange) are shown. Red arrows in Figure 2 indica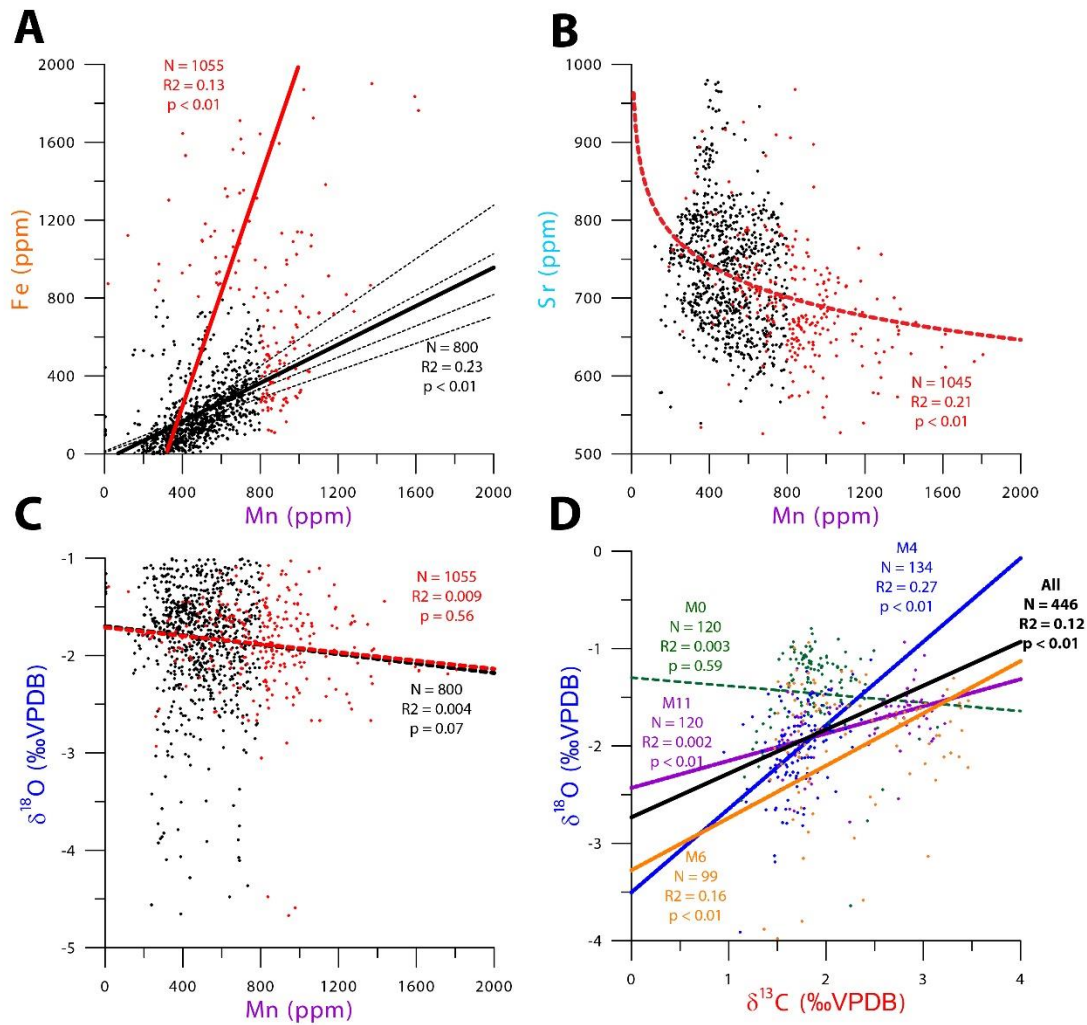te the direction of sampling. Vertical bars indicate parts of the records that were affected by diagenesis based on Mn and Fe concentrations (red bars) and stable isotope ratios (green bars). Note that the vertical scale of the Mn and Fe plots is clipped at 2000 µg/g.

Figure 6

Figure showing cross plots between trace element and stable isotope measurements in the shells. Black lines indicate correlations through all measurements, red lines show correlations of diagenetically altered samples (according to the 800 μg/g threshold for Fe and Mn) and alternatively coloured lines indicate correlations in individual shells. Statistics of the regressions are indicated in matching colours. A) [Fe] vs [Mn] showing a correlation between concentrations of these elements in all shells. Steeper slopes suggest relatively more Fe is added in diagenetically altered samples. B) [Sr] vs [Mn] showing decreasing Sr concentrations corresponding to increasing [Mn], but only in diagenetically altered samples. No significant correlation was found for pristine samples ($R^2 = 0.11$, $p = 0.25$). C) $\delta^{18}O$ vs [Mn] showing lack of correlation. D) $\delta^{18}O$ vs $\delta^{13}C$, showing positive correlation in specimens affected by diagenesis and no correlation in M0, which has pristine values.

Figure 7
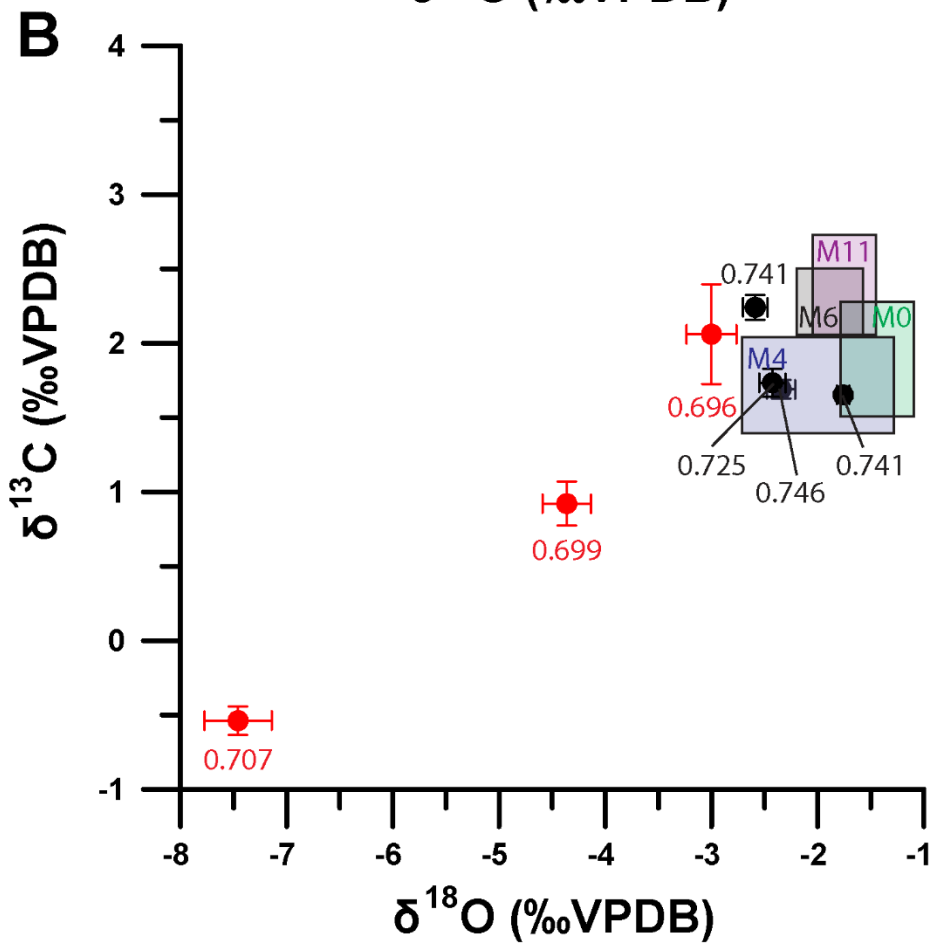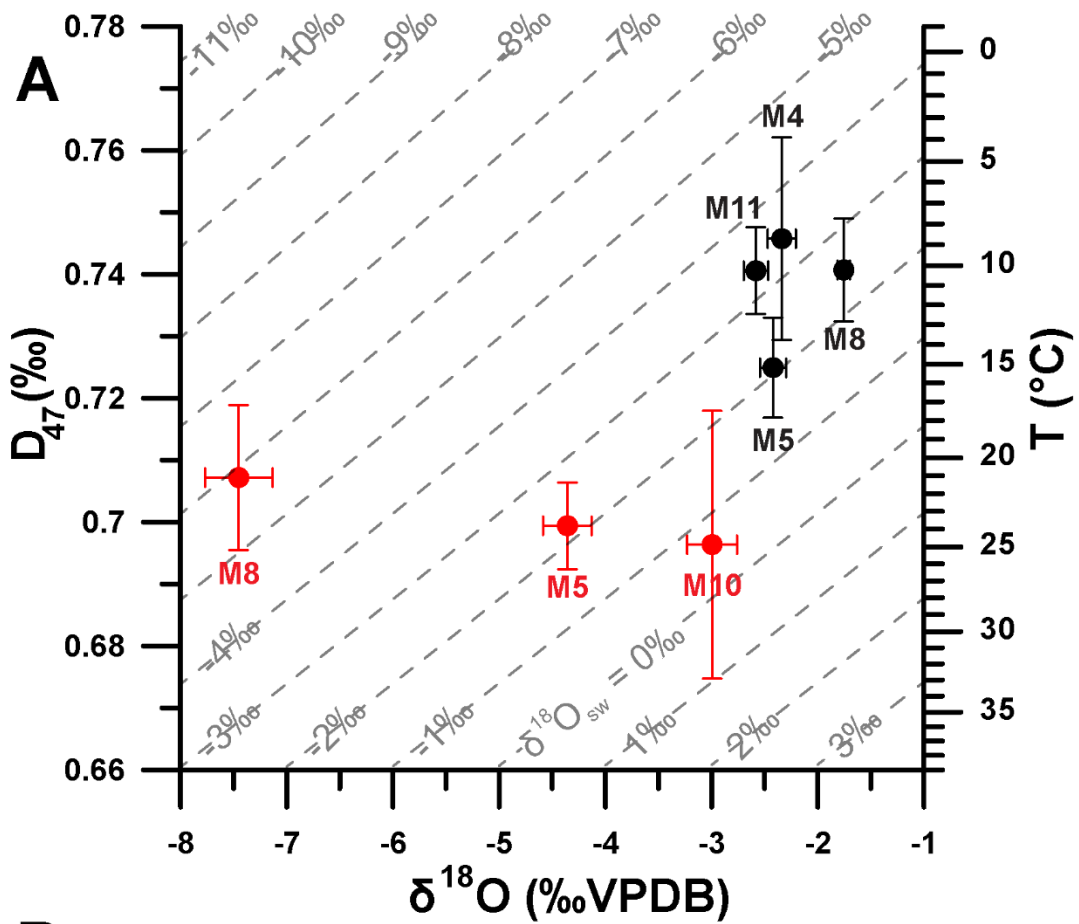
Cross plots of clumped isotope results. A) Δ_{47} vs. $\delta^{18}O$ from clumped isotope measurements on all
seven shells. Red dots and error bars represent measurements of samples from the ventral
margin of the shells, while black dots and error bars indicate results from dense foliated
calcite from the hinge of the shells. Dashed lines illustrate the $\delta^{18}O$ values of seawater that
correspond to the combination of Δ_{47} and $\delta^{18}O$ values in the graph. B) $\delta^{13}C$ vs. $\delta^{18}O$ from
clumped isotope measurements on all shells. Symbols as in A) Numbers next to the dots
indicate Δ_{47} values measured in the same samples. Coloured rectangles indicate the range of
pristine stable isotope values measured in high resolution transects through the hinges of
shells M0, M4, M6 and M11.
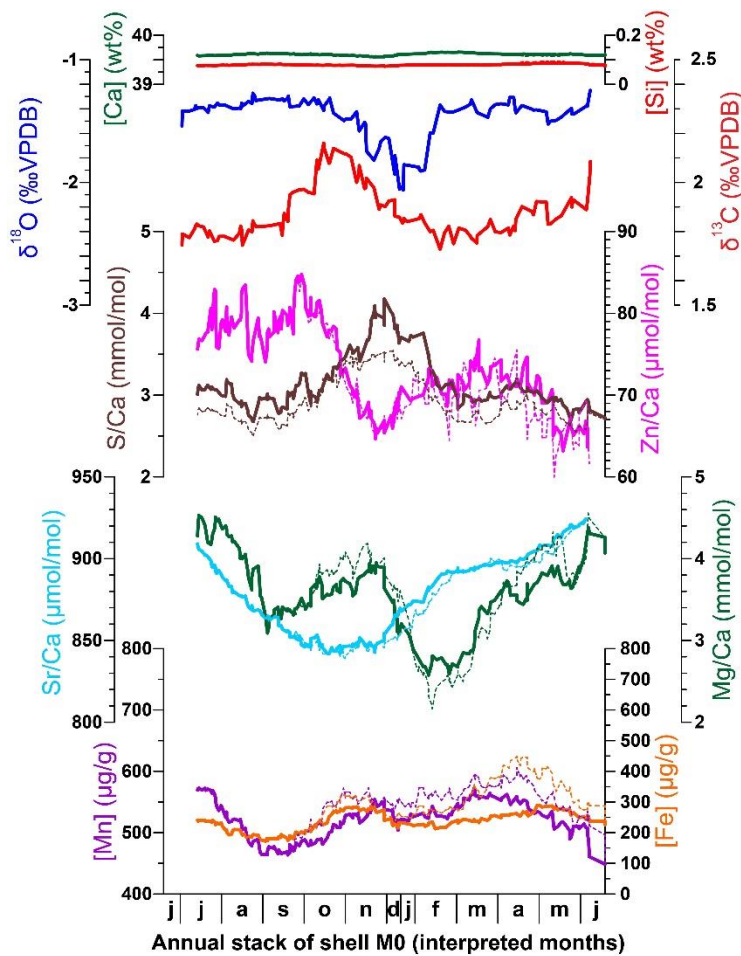
Figure 8

Stack of proxy records for shell M0 made according to a tentative interpretation of annual cyclicity
based on $\delta^{18}O$ and Sr/Ca ratios in **Figure 5**. Solid lines indicate annual stacks excluding
diagenetically altered samples while dashed lines include all measured samples to show the
effect of diagenesis. From top to bottom, stacks of [Ca] (green), [Si] (red), $\delta^{13}C$ (red), $\delta^{18}O$
(blue), S/Ca ratios (brown), Zn/Ca ratios (purple), Sr/Ca ratios (light blue), , Mg/Ca (green),
[Mn] (purple) and [Fe] (orange) records are shown. Subdivisions of the stack into months are
based on an interpretation of the phase relationship between the proxies in terms of
palaeoenvironmental seasonality. Note that summer months (December and January) are
underrepresented in the record due to the interpreted decrease or cessation of shell
growth.
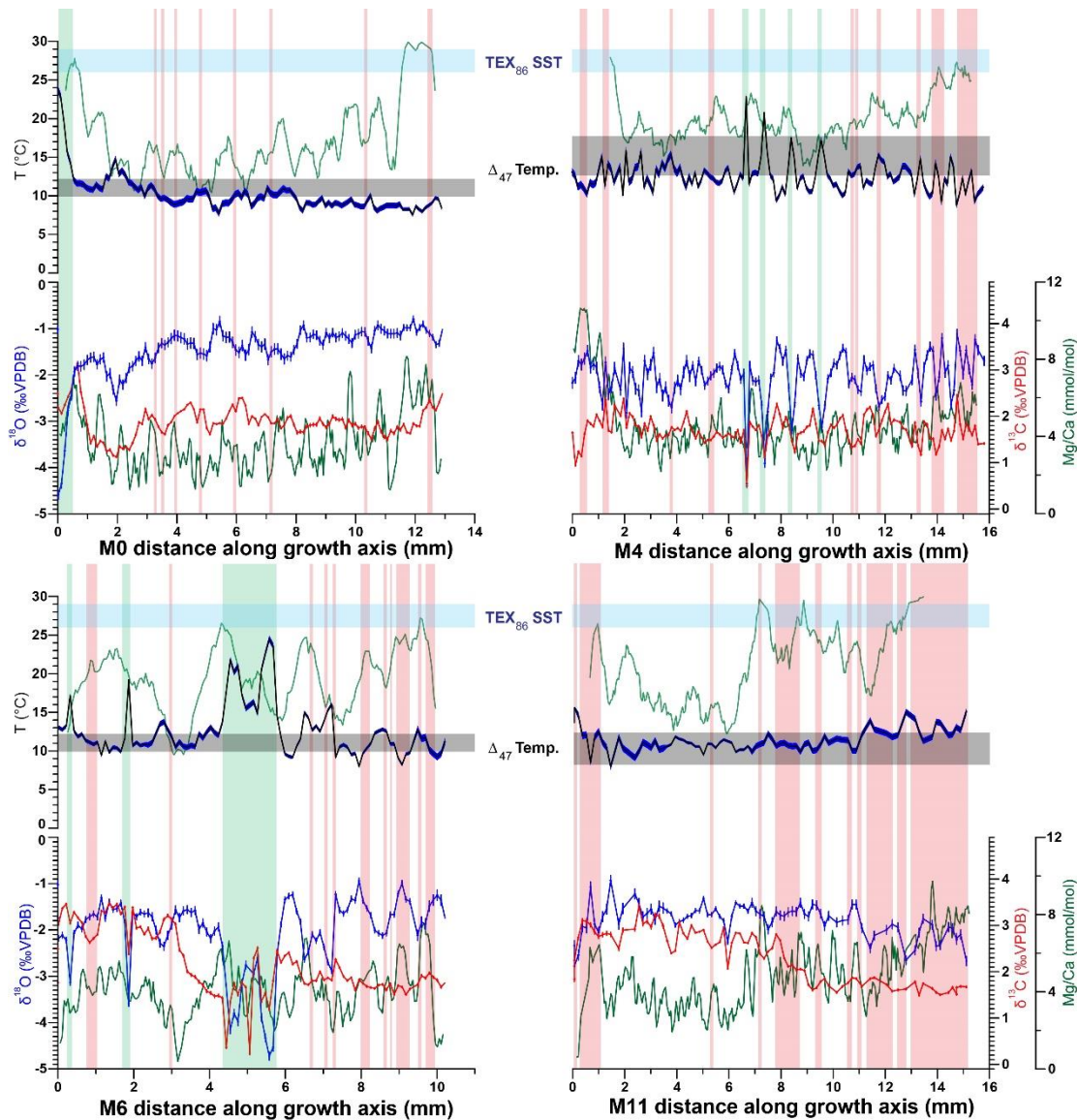
Figure 9

Overview of stable isotope and Mg/Ca records (bottom) as well as tentative temperature and salinity reconstructions (top) based on $\delta^{18}O$ (blue) and Mg/Ca (green), clumped isotope analysis (grey bars) and TEX_{86}^{H} palaeothermometry (light blue bars). Temperatures calculated from $\delta^{18}O$ records (dark blue on top) are based on the calibration by Hays and Grossman (1991) and the $\delta^{18}O_{sw}$ value of the clumped isotope measurements indicated in grey. Mg/Ca temperatures (green line on top) were calculated using the calibration reported in Surge and Lohmann (2008) with a factor 3.3 correction for lower Mg/Ca ratios in late Cretaceous ocean water. Temperatures of bulk samples of shells M4 and M11 measured using clumped isotope analysis are indicated by grey bars in graphs of M0 and M6 represent average clumped isotope temperatures of all pristine shell samples (see **Table 1**). Red and green vertical bars indicate intervals were vesicular calcite was incorporated in the stable isotopic measurements (see **Figure 5**).

Shell name	Sampling Location	N	δ13Cav (VPDB)	±1σ	δ13C_record (VPDB)	±season	δ18Oav (VPDB)	±1σ	δ18O_record (VPDB)	±season	D47av	±1σ	T_av (°C)	±1σ	δ18Osw	±1σ
M0	Shell hinge				1.91	±0.38			-1.43	±0.35						
M4	Shell hinge	3	1.74	±0.10	1.73	±0.32	-2.42	±0.12	-1.99	±0.72	0.725	±0.008	15.2	±2.6	-2.1	±0.7
M5	Shell hinge	3	1.70	±0.06			-2.34	±0.13			0.746	±0.016	9.0	±4.9	-3.4	±1.2
M6	Shell hinge				2.28	±0.23			-1.88	-±0.31						
M8	Shell hinge	4	1.66	±0.02			-1.75	±0.06			0.741	±0.008	10.3	±2.5	-2.5	±0.6
M11	Shell hinge	4	2.25	±0.08	2.40	±0.34	-2.58	±0.11	-1.74	±0.30	0.741	±0.007	10.3	±2.1	-3.3	±0.6
M5	Ventral margin	4	0.93	±0.15			-4.36	±0.23			0.699	±0.007	23.8	±2.5	-2.2	±0.7
M8	Ventral margin	4	-0.53	±0.10			-7.45	±0.32			0.707	±0.012	21.3	±4.0	-5.9	±1.1
M10	Ventral margin	3	2.07	±0.34			-2.99	±0.23			0.696	±0.022	25.4	±7.7	-0.6	±1.8
Average	Shell hinge	14									0.738	±0.004	11.1	±1.2	-2.8	±0.6
Average	Ventral margin	11									0.701	±0.007	23.3	±2.9	-3.1	±2.5

Table 1

Overview table of stable and clumped isotope results in this study. Rows highlighted in red represent samples from the ventral margin of the shells (which contain vesicular calcite). Rows with a white background represent samples of the dense foliated shell hinge. Note that for some shells (M5 and M8) both the ventral margin and the shell hinge was measured. Columns labelled "δ13C_record" and "δ18O_record" contain averages of the high-resolution stable isotope records measured in the shell hinges (if available, Figure 5). The bottom two rows contain average Δ_{47} and $\delta^{18}O_{sw}$ values of shell hinge (white) and ventral margin (red) samples, highlighting the difference between the two sampling strategies.